Acta Biomaterialia 182 (2024) 171–187

Contents lists available at ScienceDirect

Acta Biomaterialia

journal homepage: www.elsevier.com/locate/actbio

Full length article

High molecular weight hyaluronic acid-liposome delivery system for efficient transdermal treatment of acute and chronic skin photodamage

Hui Xing[a,b,1], Xiangjun Pan[a,1], Yihan Hu[a,c], Yuhui Yang[b], Ziyi Zhao[b], Huanqi Peng[b], Jianjin Wang[e], Shanying Li[e], Yunfeng Hu[a,*], Guowei Li[a,d,*], Dong Ma[b,*]

[a] The First Affiliated Hospital of Jinan University, Jinan University, Guangzhou, 510630, China
[b] Key Laboratory of Biomaterials of Guangdong Higher Education Institutes, Department of Biomedical Engineering, Jinan University, Guangzhou 510632, China
[c] Department of Cardiology, The First Affiliated Hospital of Jinan University, Guangzhou, 510630, China
[d] Department of Nuclear Medicine and PET/CT-MRI Center, The First Affiliated Hospital of Jinan University, Jinan University, Guangzhou, 510630, China
[e] Honest Medical China Co., Ltd, Zhuhai, 519000, China

ARTICLE INFO

Article history:
Received 23 February 2024
Revised 21 April 2024
Accepted 12 May 2024
Available online 15 May 2024

Keywords:
High molecular weight hyaluronic acid
Transdermal drug delivery
Liposomes
Acute photodamage
Chronic photodamage

ABSTRACT

Photodamage is one of the most common causes of skin injury. High molecular weight hyaluronic acid (HHA) has shown immense potential in the treatment of skin photodamage by virtue of its anti-inflammatory, reparative, and antioxidative properties. However, due to its large molecular structure of HHA, HHA solution could only form a protective film on the skin surface in conventional application, failing to effectively penetrate the skin, which necessitates the development of new delivery strategies. Liposomes, with a structure similar to biological membranes, have garnered extensive attention as transdermal drug delivery carriers because of their advantages in permeability, dermal compatibility, and biosafety. Herein, we have developed a HHA-liposome transdermal system (HHL) by embedding HHA into the liposome structure using reverse evaporation, high-speed homogenization, and micro-jet techniques. The effective penetration and long-term residence of HHA in skin tissue were multidimensionally verified, and the kinetics of HHA in the skin were extensively studied. Moreover, it was demonstrated that HHL significantly strengthened the activity of human keratinocytes and effectively inhibits photo-induced cellular aging *in vitro*. Furthermore, a murine model of acute skin injury induced by laser ablation was established, where the transdermal system showed significant anti-inflammatory and immunosuppressive properties, promoting skin proliferation and scar repair, thereby demonstrating immense potential in accelerating skin wound healing. Meanwhile, HHL significantly ameliorated skin barrier dysfunction caused by simulated sunlight exposure, inhibited skin erythema, inflammatory responses, and oxidative stress, and promoted collagen expression in a chronic photodamage skin model. Therefore, this transdermal delivery system with biocompatibility represents a promising new strategy for the non-invasive application of HHA in skin photodamage, revealing the significant potential for clinical translation and broad application prospects.

Statement of significance

The transdermal system utilizing hyaluronic acid-based liposomes enhances skin permeability and retains high molecular weight hyaluronic acid (HHL). *In vitro* experiments with human keratinocytes demonstrate significant skin repair effects of HHL and its effective inhibition of cellular aging. In an acute photodamage model, HHL exhibits stronger anti-inflammatory and immunosuppressive properties, promoting skin

* Corresponding authors.
E-mail addresses: huyunfeng@jnu.edu.cn (Y. Hu), liguowei@jnu.edu.cn (G. Li), tmadong@jnu.edu.cn (D. Ma).
[1] H.X. and X.P. contributed equally to this work.

https://doi.org/10.1016/j.actbio.2024.05.026

proliferation and scar repair. In a chronic photodamage model, HHL significantly improves skin barrier dysfunction, reduces oxidative stress induced by simulated sunlight, and enhances collagen expression.

1. Introduction

The skin, serving as the body's first line of defense, is frequently subjected to physical, chemical, and biological assaults. With human activities contributing to the depletion of the ozone layer, acute and chronic photodamage has become one of the most common causes of skin injury [1]. Photodamage induces the release of a large number of free radicals within the skin, leading to oxidative stress, immune responses, and the loss of collagen [2]. Currently, most treatments for damaged skin, such as local injections, microneedle therapy, and photodynamic therapy, are invasive and can easily lead to secondary skin damage [3]. The transdermal drug delivery system (TDDS), known for avoiding first-pass metabolism, non-invasive administration, and high efficiency, is hailed as one of the most promising non-invasive drug delivery methods [4]. However, the stratum corneum, as the most crucial protective structure of the skin, acts like a semipermeable membrane, posing a formidable barrier to most drugs due to its selective permeability [5]. In recent years, with continuous advancements in research, various techniques have been employed to improve transdermal or topical drug delivery, including the use of chemical enhancers, iontophoresis, electroporation, and others [6]. Therefore, in the research and application of TDDS for damaged skin, selecting an appropriate transdermal enhancement strategy that balances safety and efficacy remains a key focus and challenge in current studies [7].

Hyaluronic acid (HA) is a unique natural linear polysaccharide characterized by its specific high molecular structure and a variety of biological functions, including high biocompatibility, good biodegradability, and significant bioactivity [8]. In TDDS, HA serves a dual purpose: on one hand, it increases the water content of the stratum corneum to enhance permeation; on the other hand, due to its hydrophobic plate-like domains containing CH groups, it exhibits amphiphilicity, enabling it to form complexes with phospholipids to further facilitate permeation [9]. In the treatment of skin injuries, high molecular weight hyaluronic acid (HHA) demonstrates superior anti-inflammatory, antioxidant, and repair properties compared to low molecular weight HA (LHA). However, LHA, which more readily penetrates the skin, is quickly degraded due to oxidants and hyaluronidases in the skin, failing to provide long-lasting effects. In contrast, HHA, with its multiple repeating units, is often administered via injection due to its structural characteristics. Conventional topical application merely forms a protective film on the outer layer of the skin and struggles to penetrate the skin layers to repair damage or provide transdermal filling effects [10-13]. Therefore, developing a new type of transdermal system that enables efficient penetration and prolonged residency of HHA in the skin, thereby enhancing the utilization of HHA, has become an urgent priority.

Liposomes, with their high biocompatibility, low toxicity, and high encapsulating properties, have become a widely researched and utilized drug delivery system. This artificial membrane system serves as a favorable carrier for promoting the transdermal delivery of amphiphilic, insoluble, and large-molecule drugs, finding extensive applications in immune therapy, skin, pulmonary, and oral drug delivery [14,15]. The preparation methods of lipid carriers are relatively mature, including traditional thin-film hydration, ethanol injection, reverse evaporation, as well as freeze-drying, supercritical fluid, microfluidics, and other new technologies [16-18]. As a delivery vehicle for transdermal administration, it also possesses numerous advantages. For example, Wu et al. developed a thermosensitive hydrogel liposome for sustained transdermal delivery, which reduced melanin deposition and lipid peroxidation, significantly enhancing the skin's anti-photoaging properties [19]. Our team previously developed an ethosome containing HA (HA-ES), exploring the advantages of hyaluronic acid in enhancing transdermal delivery. This provided a rapid, efficient, safe, and self-administrable transdermal drug delivery system [5]. Additionally, we have recently developed a nitric oxide-based liposome, which, by incorporating nitric oxide, enhances permeation and synergistic therapeutic functions on top of the inherent advantages of the liposome itself [20]. Therefore, leveraging the benefits of both liposomes and HA to construct a HHA transdermal delivery carrier offers a promising direction for the treatment of acute and chronic photodamaged skin.

Based on the discussions above, this study successfully embedded hyaluronic acid into the structure of liposomes using reverse-phase evaporation, high-speed homogenization, and microjet high-pressure methods, transforming it into a component of the liposome, thus forming a hyaluronic acid liposome (HL). Initially, we conducted a detailed analysis of the structural characteristics and stability of HL using various methods and tracked the dynamic distribution and penetration behavior of hyaluronic acid in skin tissue through fluorescence labeling and *in vivo* imaging. It was demonstrated that different molecular weights, especially HHA, possess an enhanced permeation and retention effect (EPR), potentially significantly improving the utilization of HHA. *In vitro* experiments on human keratinocytes showed that, compared to LHA, HHA exhibited stronger proliferation-promoting and anti-aging effects. Building on these findings, we established an acute photodamage model generated by a laser ablation technique. During the treatment process, high molecular weight hyaluronic acid liposome (HHL) effectively inhibited the expression of inflammatory factors and promoted the production of proliferation factors, creating a favorable microenvironment for damaged skin. This demonstrated significant potential in accelerating skin regeneration and scar repair. A chronic photodamage animal model was also constructed, during the skin barrier dysfunction induced by simulated sunlight, HHL significantly inhibited skin erythema, inflammatory responses, and alleviated lipid peroxidation in the skin, promoting collagen expression, aiming to achieve integrated protective and therapeutic effects. Finally, a detailed evaluation of the material's biosafety confirmed its biocompatibility. Therefore, this transdermal delivery system offers a viable approach for the non-invasive application of HHA in acute and chronic damaged skin, holding significant potential for clinical translation and broad application prospects. The abbreviation used in this study was presented in Table 1.

2. Materials and methods

2.1. Materials preparation

Soybean lecithin (CAS:8002–43–5) was purchased from Aladdin Biochemical Technology Co., Ltd. (Shanghai, China). Cholesterol (Cho, CAS: 57–88–5) was obtained from Qiyun Biotechnology Co., Ltd. (Guangzhou, China). Sodium hyaluronate (CAS: 9067–32–7) and 5-amino fluorescein (CAS: 27,599–63–9) were acquired from Jinsui Bio-Technology Co., Ltd. (Shanghai, China). Anhydrous

Table 1
Sample list of the abbreviation used in this study.

Sample description	Abbreviation
High molecular weight hyaluronic acid	HHA
HHA-liposome transdermal system	HHL
LHA-liposome transdermal system	LHL
Transdermal drug delivery system	TDDS
Hyaluronic acid	HA
Low molecular weight HA	LHA
Ethosome containing HA	HA-ES
Hyaluronic acid liposome	HL
Enhanced permeation and retention effect	EPR
5-amino fluorescein	5AF
Polydispersity index	PDI
Sodium alginate	SA
Enzyme-linked immunosorbent assay	ELISA
3,3′,5,5′-Tetramethylbenzidine	TMB
4′,6-diamidino-2-phenylindole	DAPI
Minimum erythemal dose	MED
Transmission electron microscopy	TEM
Human immortalized keratinocytes	HaCat
Elastic van gieson	EVG
Extracellular matrix	ECM

ethanol (AR) was sourced from Guangzhou Chemical Reagent Factory (Guangzhou, China). DMEM, trypsin, fetal bovine serum, penicillin-streptomycin double antibiotic solution were procured from Gibco (USA). CCK-8 assay kit, β-galactosidase assay kit, CAT assay kit, SOD assay kit, MDA assay kit were purchased from Beyotime Institute of Biotechnology (Shanghai, China). Mouse anti-Ki67, VEGF, IL-6, IL-1β, TNF-α, MMP3 antibodies were bought from Servicebio Technology Co., Ltd. (Wuhan, China). Human immortalized keratinocytes (HaCat) were obtained from Meisen Cell Technology Co., Ltd. (Zhejiang, China).

2.2. Research on the preparation process of hyaluronic acid liposome

2.2.1. Labeling of hyaluronic acid

Fluorescence labeling was used to label HA of four different molecular weights (3 k, 150–250 k, 400–1000 k, 1–1.5 m) [5]. Different molecular weights of HA, EDC–HCl, and NHS were added to pure water in a molar ratio of 1:1.2:1.2. The solution was stirred to activate the carboxyl groups of HA for 4 h. 5-amino fluorescein (5AF) was then added to the above solution and stirred for 24 h before dialysis in pure water. The mass ratio of HA to 5AF was set at 10:1. The dialysis process involved multiple water changes until no fluorescein was detected in the effluent. The labeled hyaluronic acid was freeze-dried to obtain HA-5AF powder of four different molecular weights. The entire experiment was conducted in a light-avoiding environment.

2.2.2. Preparation of HA-5AF liposomes

The HA-5AF liposomes were innovatively prepared using reverse-phase evaporation technology combined with high-speed homogenization and micro-jet high-pressure techniques. Briefly, four types of HA-5AF powders (0.1 %, w/v) were precisely weighed and added to phosphate buffer solution (PBS, pH = 7.4). The mixture was stirred for 4 h to ensure complete dissolution of HA-5AF into the solution. A certain amount of soybean lecithin (1 %, w/v) and cholesterol (0.06 %, w/v) were then weighed and added to anhydrous ethanol. This mixture was heated in a water bath until fully dissolved, followed by stirring to ensure uniform mixing. Subsequently, the HA-5AF solution was added and emulsified using a high-shear dispersing emulsifier until a stable water-in-oil (W/O) emulsion was formed. The ethanol in the emulsion was then removed under a rotary evaporator, and the temperature was reduced to room temperature. A certain amount of PBS (pH = 7.4) was added, and the mixture was homogenously stirred. The resultant HA-5AF liposome assemblies were then passed through a 450 nm polycarbonate membrane, forming primary HA-5AF liposome assemblies. These primary assemblies were slowly added to a certain volume of PBS (pH = 7.4) and emulsified again using a high-shear dispersing emulsifier until stable. The resulting hyaluronic acid liposome assemblies were then processed through a micro-jet high-pressure homogenizer, repeating the process twice to obtain stable final HA-5AF liposomes. The same operational steps were followed to obtain hyaluronic acid liposomes without 5AF.

2.2.3. Characterization

The particle size, ζ-potential and polydispersity index (PDI) variation of the hyaluronic acid liposomes were measured using a laser nanoparticle size analyzer (Malvern, Malvern Panalytical Ltd, Worcester). The distribution of 5AF-labeled hyaluronic acid within the liposome structure was characterized using a laser scanning confocal microscope (LSM 880). The morphological changes of hyaluronic acid liposomes with different molecular weights were observed using a high-resolution transmission electron microscope (JEOL TEM-1210) operating at a working voltage of 120 kV.

2.3. Skin kinetics analysis of hyaluronic acid liposomes

2.3.1. Establishment of HA-5AF standard curve

The procedure is briefly described as follows: First, different concentrations of HA-5AF liposomes (ranging from 0 to 20 μg/mL) were prepared. The standard curves for HA-5AF liposomes of the four molecular weights were plotted using a multifunctional enzyme reader (Synergy H1) and the characteristic absorbance of 5AF at 486 nm [21]. The absorbance at different concentrations was recorded to establish the corrected standard curves. These curves were then subjected to linear regression analysis using Origin 2021 software.

2.3.2. Quantitative analysis of in vitro simulated skin permeation

For this study, a Franz diffusion cell with a permeation area of 1.767 cm^2 was used to perform *in vitro* simulated skin permeation experiments with HA-5AF liposomes [22]. The receiver chamber was filled with phosphate buffer solution (pH = 7.4) and continuously stirred at a speed of 200 rpm/min. A circulating water bath maintained a constant temperature of 37 °C in the diffusion cell. Appropriate-sized mouse skin was clamped between the donor and receiver chambers, with the stratum corneum facing the donor chamber. 2 mL of freshly prepared HA-5AF liposomes of four different molecular weights and HA-5AF solution of 1–1.5 m molecular weight (with a hyaluronic acid concentration of 0.1 %) were applied to the skin in the donor chamber. At designated time intervals of 1 hour and 3 h, 1 mL of receptor solution was sampled through the sampling port and replaced with an equal volume of fresh buffer (pH = 7.4). This experiment was repeated three times, and the average value was taken. The content of hyaluronic acid in the receptor solution was analyzed by measuring the absorbance at 486 nm using a multifunctional enzyme reader (Synergy H1) [23].

2.3.3. Analysis of skin permeation depth and distribution

After conducting the *in vitro* permeation experiment using the Franz diffusion cell for 3 h, the excess sample solution was removed. The skin was then taken out from the Franz diffusion cell and washed three times with distilled water to ensure that no sample residues remained on the skin surface. The skin tissue was dried with gauze and cut into small pieces approximately 1 cm^2 in size, then embedded with cryoembedding medium (OCT compound) and stored at −80 °C for solidification. Subsequently, the frozen skin tissues were sectioned vertically into slices approximately 10 μm thick at −20 °C using a cryostat. These skin tissue slices were then placed on microscope slides and observed using an AxioCamMRc inverted fluorescence microscope.

2.3.4. In vivo *permeation experiment*

After anesthetizing the mice, the hair in a uniform area on each mouse's back was removed using a shaver and depilatory cream to eliminate interference with fluorescence imaging. Then, 100 μL of HA-5AF liposome suspension of molecular weights 3 k and 1–1.5 m were gently applied to the mice's backs. The distribution of fluorescence was observed using a small animal *in vivo* imaging system (FX Pro). After allowing complete absorption for 2 h, the dorsal skin tissues were removed. Fluorescence measurements were then performed on the subcutaneous muscle tissue of the mice using the *in vivo* imaging system to determine whether hyaluronic acid had penetrated the skin. The proportion of penetrated HA was quantitatively analyzed through fluorescence. The excised skin tissues were then embedded, frozen, sectioned, and observed for the distribution of liposomes using an AxioCamMRc inverted fluorescence microscope.

2.3.5. Transdermal study of large molecular substances as alternatives to hyaluronic acid

Sodium alginate (SA) with viscosities of 15 and 200 mPa·s was labeled using the previous method [24]. The procedure is briefly described as follows: First, sodium alginate (1 %, w/v) was dissolved in distilled water, and a few drops of concentrated sulfuric acid were added to precipitate the alginate. The mixture was centrifuged (8000 rpm/min) to collect the alginate precipitate, which was then washed with water and acetone. The washed particles were dried overnight in a vacuum in the presence of phosphorus pentoxide. The dried alginate was then stirred with 50 mg of 5-amino fluorescein, 1 g EDC, 30 mL 1,4-dioxane, and 80 mL distilled water until it turned orange, followed by washing with acetone to remove unreacted alginate. The washed particles were dried in a vacuum and then used for the preparation of SA-5AF liposomes and *in vivo* permeation experiments to verify that this liposome preparation technique can effectively enable the permeation of large molecular substances. The experimental operations were the same as those described above.

2.4. Effect of high molecular weight hyaluronic acid on human keratinocytes

2.4.1. HaCat proliferation experiment

HaCat cells were cultured in DMEM supplemented with 10 % fetal bovine serum (v/v) and 1 % antibiotics (v/v) [25]. The cells were seeded in a 96-well plate at a density of 5×10^3 cells per well and incubated at 37 °C in a 5 % CO_2 environment for 24 h. After this incubation period, the medium was removed and replaced with liposomes without hyaluronic acid and with the same concentration of hyaluronic acid in LHA, HHA, LHL, and HHL (each sample containing 0.01 % hyaluronic acid). The control group was cultured only in the medium. Each group had three parallel wells. After an additional 24 h of culture, the material was removed and CCK-8 reagent was added. The absorbance at 450 nm was recorded using a multifunctional enzyme reader to calculate the cell proliferation rate after treatment with different materials [26].

2.4.2. Migration experiment

The effect of materials on cell migration was assessed using the scratch assay [27]. The procedure is summarized as follows: HaCat cells were seeded in a 6-well plate at a concentration of 2×10^5 cells per well. When cells reached 80 %–90 % confluence, a straight scratch was made in the center of the well. Then, liposomes without hyaluronic acid and with the same concentration of hyaluronic acid in LHA, HHA, LHL, and HHL (each sample containing 0.01 % hyaluronic acid) were added, with the medium serving as the control group. Images of cell migration were captured using an inverted microscope 12 and 24 h after treatment. Image J software was used to quantify the width of the scratch and calculate the healing rate.

2.4.3. SA-β-gal histochemical staining

Based on previous research, a photodamage cell model was established using ULTRA-VITALUX lamps with an energy of 100 mJ/cm^2, positioned 10 cm away from the cells [28]. During irradiation, PBS was used in place of the complete culture medium, and then cells were cultured in serum-free H-DMEM for 24 h. To study the antioxidative effects of the materials, photodamaged cells were treated in serum-free H-DMEM with the same concentration of hyaluronic acid in LHA, HHA, LHL, and HHL (each sample containing 0.01 % hyaluronic acid). Cells were then washed with PBS and fixed in 4 % paraformaldehyde for 5 min. SA-β-gal staining was performed using a β-galactosidase staining kit. Use an optical microscope to observe blue-stained senescent cells in three random fields.

2.5. Therapeutic application in acute photodamage animal model

2.5.1. Establishment of acute skin damage model with laser ablation

35 female BALB/C mice (6 to 8 weeks old, averaging 20 g in weight) were purchased from the Beijing Vital River Laboratory Animal Technology Co., Ltd. (Beijing, China). The animals were maintained under controlled conditions of 22 °C-24 °C room temperature, 60 % relative humidity, and a 12-hour light/dark cycle, with sufficient food and water provided throughout the experimental period. The mice were acclimatized to the experimental environment for one week prior to the experiments. Animal experiments were conducted in accordance with the ethical guidelines of the Animal Ethics Committee of Jinan University (Animal Ethics Number: IACUC-20,220,518–03). The model was established to simulate human skin laser ablation. After depilation with depilatory cream for 24 h, an acute mouse skin photodamage model was induced using a CO_2 laser ablation device (KeYing Laser). The laser ablation energy was set at 2.5 mJ/g, with an ablation area of 10×15 mm, and the procedure was repeated once.

2.5.2. Kinetic analysis of hyaluronic acid in photodamaged skin

In this experiment, the penetration of hyaluronic acid into photodamaged skin was traced transdermally using LHA, HHA, LHL, and HHL labeled with 5-amino fluorescein. During the treatment process, the mice were kept in a dark environment to prevent fluorescence quenching. The method of inducing photodamage was consistent with the previously described procedure. 12 h after administering the treatment, the mice were euthanized, and the dorsal skin was harvested. The penetration of hyaluronic acid was observed at 0 and 12 h using an *in vivo* imaging system, and the proportion of penetrated hyaluronic acid was quantitatively analyzed through fluorescence. The skin tissues were fixed in 4 % paraformaldehyde, sectioned by cryostat, and the penetration of fluorescently labeled hyaluronic acid in the tissues was observed using an AxioCamMRc inverted fluorescence microscope.

2.5.3. Skin repair and histological evaluation in mice

The experimental steps are summarized as follows: The experimental mice were divided into six groups: healthy group (Healthy), model group (Control), 3 k molecular weight hyaluronic acid (LHA) group, 1–1.5 m molecular weight hyaluronic acid (HHA) group, 3 k molecular weight hyaluronic acid liposome (LHL) group, and 1–1.5 m molecular weight hyaluronic acid liposome (HHL) group, with five mice in each group. The healthy group received no treatment, while the model group was treated with phosphate buffer solution starting from the first day after model establishment. The LHA, HHA, LHL, and HHL groups began receiving treatment and continued for 7 days. The back wounds of the mice were photographed on days 1, 3, 5, and 7 to track the healing process.

Dermoscopy was used for localized observation and recording, and the mice's weight and changes in back skin injuries were meticulously recorded. After the experiment, the healed skin tissues from the backs of the mice in each group were harvested and fixed in 4 % paraformaldehyde solution. The tissues were then embedded in paraffin, solidified, and sectioned into 5 μm thickness. H&E, Masson, and immunohistochemical staining (anti-Collagen-3, anti-CK-5) were used to observe histological changes in the skin tissues. Image J software was utilized to measure the thickness of the skin and the volume fraction of related proteins in each group. The epidermal thickness, collagen volume fraction, or protein expression intensity for each sample was calculated as the average of three random points within the sample.

2.5.4. Enzyme-linked immunosorbent assay (ELISA) of mouse skin tissues

The experimental steps are briefly described as follows: A sandwich enzyme-linked immunosorbent assay (ELISA) technique was used according to the instructions of the kit [29]. Specific antibodies against mouse IL-6, IL-1β, and TNF-α were pre-coated onto high-affinity ELISA plates. Standards, test samples, and biotinylated detection antibodies were added to the wells of the ELISA plate and incubated. IL-6, IL-1β, and TNF-α present in the samples bound to both the solid-phase antibodies and the detection antibodies. After incubation, unbound substances were removed by washing, and horseradish peroxidase-labeled streptavidin was added. Following another washing step, the chromogenic substrate TMB (3,3′,5,5′-Tetramethylbenzidine) was added for color development in a light-protected environment. The intensity of the color reaction is directly proportional to the concentration of IL-6, IL-1β, and TNF-α in the samples. The reaction was stopped by adding a stop solution, and the absorbance was measured at a wavelength of 450 nm.

2.5.5. Immunofluorescence staining of mouse skin tissues

The experimental steps are summarized as follows: The skin tissues from each group, post-treatment, were embedded in paraffin and sectioned. These sections then underwent antigen retrieval and were blocked in mouse serum for 30 min. The sections were subsequently treated with primary and secondary antibodies and incubated overnight at 4 °C. 4′,6-diamidino-2-phenylindole (DAPI) was used to counterstain the cell nuclei. Fluorescent characteristics were observed using the fluorescent mode of a Leica M165 FC microscope, and the fluorescence intensity was measured using Image J software.

2.5.6. Terminal deoxynucleotidyl transferase dUTP nick end labeling (TUNEL) staining

The TUNEL staining method involves labeling the 3′-ends of DNA with fluorescein-conjugated dUTP. This allows for the observation of apoptotic cells under a fluorescence microscope. The paraffin-embedded skin sections prepared as mentioned above were stained using a TUNEL staining kit [30]. This process enables the visualization of apoptotic cells in the epidermis using an Axio-CamMRc inverted fluorescence microscope.

2.6. Therapeutic application in chronic photodamage animal model

2.6.1. Establishment of chronic skin damage model simulating sunlight exposure

35 female BALB/C nude mice (6 to 8 weeks old, averaging 20 g in weight) were purchased from Beijing Vital River Laboratory Animal Technology Co., Ltd. (Beijing, China). The animals were maintained under controlled conditions of 22 °C-24 °C room temperature, 60 % relative humidity, and a 12-hour light/dark cycle, with sufficient food and water provided throughout the experimental period. The mice were acclimatized to the experimental environment for one week prior to the experiments. Animal experiments were conducted in accordance with the ethical guidelines of the Animal Ethics Committee of Jinan University (Animal Ethics Number: IACUC-20230913–01).After acclimatization, the mice were divided into seven groups: healthy group (Healthy), model group (Control), positive control with Vitamin A cream (AC) group, 3 k molecular weight hyaluronic acid (LHA) group, 1–1.5 m molecular weight hyaluronic acid (HHA) group, 3 k molecular weight hyaluronic acid liposome (LHL) group, and 1–1.5 m molecular weight hyaluronic acid liposome (HHL) group, with five mice in each group. The experimental procedure followed previous steps with some modifications [31]. All mice, except those in the healthy group, were irradiated with an ULTRA-VITALUX lamp (Osram, Germany). The lamp was turned on for 2 min before irradiation to stabilize the light source. The irradiation position was set 30 cm below the lamp, and the irradiation intensity was confirmed by the radiometer. The mice were placed in the irradiation position, back facing up, and fixed with a mouse restrainer to fully expose the skin to be irradiated. The minimum erythemal dose (MED) was determined through a preliminary experiment, with reference to previous literature [32]. After establishing the MED, the naked mice were irradiated for 8 weeks, four times per week. The first week's irradiation was at 0.5 MED, increasing by 0.5 MED each week until reaching 2 MEDs by the fourth week, and then maintaining 2 MEDs until the end of the 8th week, totaling 52 MEDs, treatment began on the first day of the experiment. The Healthy group received no treatment, while the Control group was treated with phosphate buffer solution (pH = 7.4), continuing for 8 weeks. The back of the mice was photographed every 15 days to track changes, with further localized observation using a dermoscopy. Mouse weight and changes in back skin were meticulously recorded. After the experiment, the skin tissues from the backs of the mice in each group were harvested and fixed in 4 % paraformaldehyde solution. The tissues were then embedded in paraffin, solidified, and sectioned into 5 μm thickness. H&E, Masson, Verhoeff, and immunohistochemical staining (anti-MMP3) were used to observe histological changes in the skin tissues. Image J software was utilized to measure related indicators.

2.6.2. Enzyme-linked immunosorbent assay (ELISA) of mouse skin tissues

The experimental steps are briefly described as follows: A sandwich enzyme-linked immunosorbent assay (ELISA) technique was used according to the instructions provided with the kit. Specific antibodies against mouse IL-6, TNF-α, IL-1β, SOD (Superoxide Dismutase), CAT (Catalase), and MDA (Malondialdehyde) were pre-coated onto high-affinity ELISA plates [29]. Standards, test samples, and biotinylated detection antibodies were added to the wells of the ELISA plate and incubated. IL-6, TNF-α, IL-1β, SOD, CAT, and MDA present in the samples bound to both the solid-phase antibodies and the detection antibodies. After incubation, unbound substances were removed by washing, and horseradish peroxidase-labeled streptavidin was added. Following another washing step, the chromogenic substrate TMB (3,3′,5,5′-Tetramethylbenzidine) was added for color development. The intensity of the color reaction is directly proportional to the concentration of IL-6 (450 nm), TNF-α (450 nm), IL-1β (450 nm), SOD (550 nm), CAT (405 nm), and MDA (532 nm) in the samples. The reaction was stopped by adding a stop solution, and the absorbance was measured at different wavelengths.

2.6.3. Western blotting analysis

The total protein from the skin was extracted using a Total Protein Extraction Kit, followed by ultracentrifugation and ultrasonica-

tion. The protein suspension was mixed with protein loading buffer in a 4:1 vol ratio and boiled for 10 min. The protein expression was detected according to the method previously reported [33]. A dilution ratio of 1:1000 was used for anti-NF-κB antibody and anti-GAPDH antibody as an internal control for protein expression. After incubation, the samples were analyzed using a chemiluminescence imaging system (ChemiDoc MP, Bio-Rad, USA).

2.7. Biocompatibility analysis

2.7.1. Skin sensitization test

To assess the irritation and sensitization of the materials on mouse skin, the behavioral activities and general health of the mice were observed after three consecutive days of topical application on the dorsal skin. Additionally, dermatoscopy was employed to record the treated skin areas of mice in each group, observing for symptoms like skin peeling, scab formation, and edema.

2.7.2. In vivo *toxicity*

After the treatment of the aforementioned animal models was completed, the mice in each group were euthanized. The heart, liver, spleen, lungs, and kidneys were harvested, rinsed multiple times with PBS (pH = 7.4) to remove blood stains, and then immersed in tissue fixative. Subsequently, the tissues were embedded in paraffin, sectioned, and stained with Hematoxylin and Eosin (H&E). These sections were observed and photographed using an upright microscope (Motic). In addition, blood samples were collected from the mice, and serum was obtained through centrifugation for further biochemical analysis.

2.8. Statistical analysis

All data were presented as mean ± standard deviation (SD). Differences between experimental groups were analyzed using the One-way ANOVA method in GraphPad Software (Inc., La Jolla, CA, USA). The significance of differences was determined based on P-values, where $^{*}P < 0.05$; $^{**}P < 0.01$; $^{***}P < 0.001$; $^{****}P < 0.0001$ indicate levels of statistical significance.

3. Results and discussions

3.1. Preparation and characterization of hyaluronic acid liposomes (HL)

In this study, hyaluronic acid liposomes (HL) of different molecular weights were successfully prepared using high-shear dispersion and micro-jet high-pressure techniques, combined with reverse-phase evaporation, and were characterized in detail (the preparation process is shown in Fig. 1a).

First, the size and zeta potential changes of HL with different molecular weights were shown in Fig. 1b. The hydrated particle sizes of HL were all below 500 nm, which were 324.1 ± 36.94, 352.23 ± 9.09, 362 ± 18.09, and 339.97 ± 6.45 nm respectively, indicating that these liposomes have a sufficiently small size to penetrate the skin [34]. Simultaneously, with the increase in molecular weight, the electrical potential of HL exhibits a downward trend. Zeta potential, as a parameter measuring the velocity of charged particle movement in solution, is associated with the charge and size of particles in the solution. For hyaluronic acid (HA), higher molecular weight HA molecules, composed of more units, carry more negative charges, resulting in a higher charge density in the solution, thereby increasing the Zeta potential. A larger absolute value of Zeta potential indicates that charged particles in the dispersion system are more uniformly dispersed in the solvent, making aggregation or precipitation less likely to occur. This contributes to maintaining the uniformity and stability of the dispersion system [35-38].

Further, Transmission electron microscopy (TEM) was used to observe the morphology of HL. As shown in Fig. 1c, the hyaluronic acid liposomes of different molecular weights appeared as round,

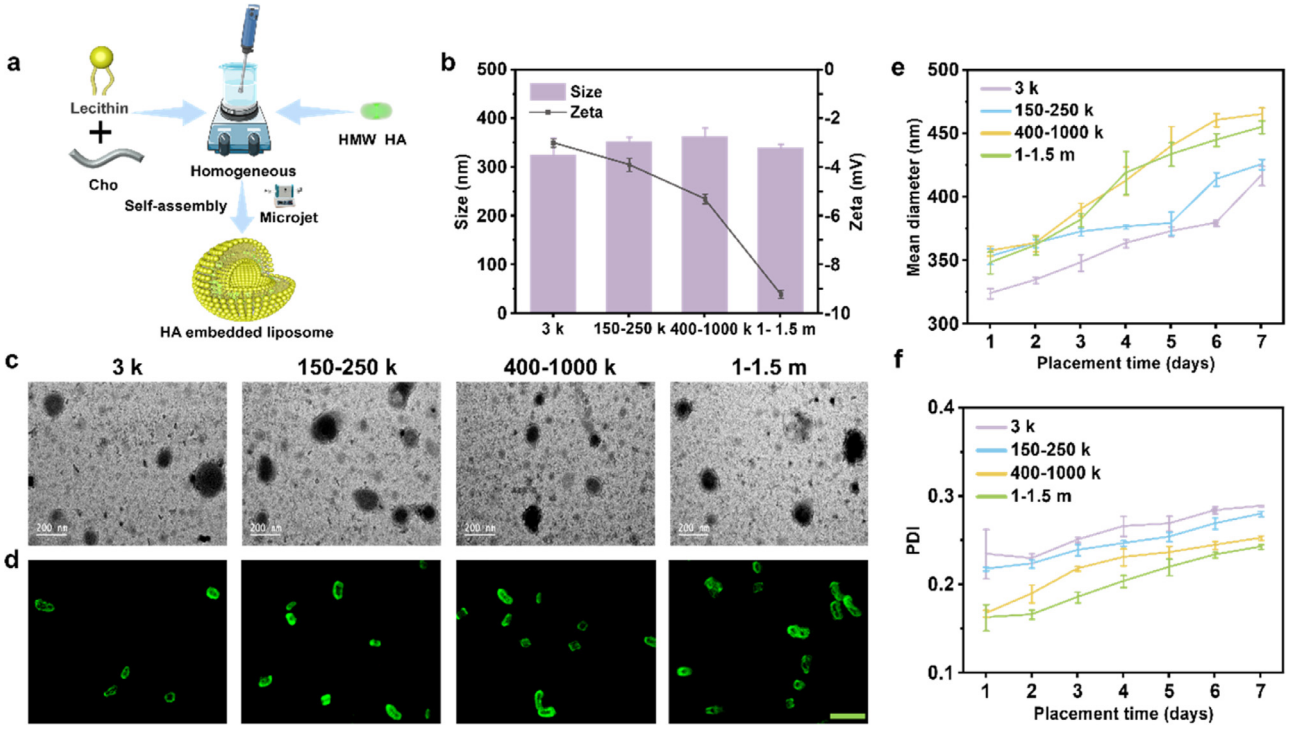

Fig. 1. Synthesis and Characterization of HL. (a) Schematic representation of HL synthesis. (b) Particle size and zeta potential of HL with molecular weights of 3 k, 150–250 k, 400–1000 k, and 1–1.5 m. (c) TEM images of HL with molecular weights of 3 k, 150–250 k, 400–1000 k, and 1–1.5 m; scale bar = 200 nm. (d) Localization of HA in liposomes; scale bar = 1 μm. (e) Stability of particle size over seven days for HL with molecular weights of 3 k, 150–250 k, 400–1000 k, and 1–1.5 m. (f) The PDI over seven days for HL with molecular weights of 3 k, 150–250 k, 400–1000 k, and 1–1.5 m.

enclosed vesicular structures with no significant morphological changes, and the dried size stabilized at around 100 nm with uniform particle size distribution. To represent the composition and morphological structure of HL more intuitively, 5-amino fluorescein (5AF) was used to fluorescently label the hyaluronic acid in the liposomes. Tracking and recording of the position of hyaluronic acid in the liposomes, the Fig. 1d showed that HL appeared as hollow ring structures, with HA participating in the assembly of the liposomes, evenly embedded within, and forming a stable ring structure, the structure is similar to our previous study [20].

Additionally, the long-term stability of liposomes is an important indicator for their clinical application in transdermal drug

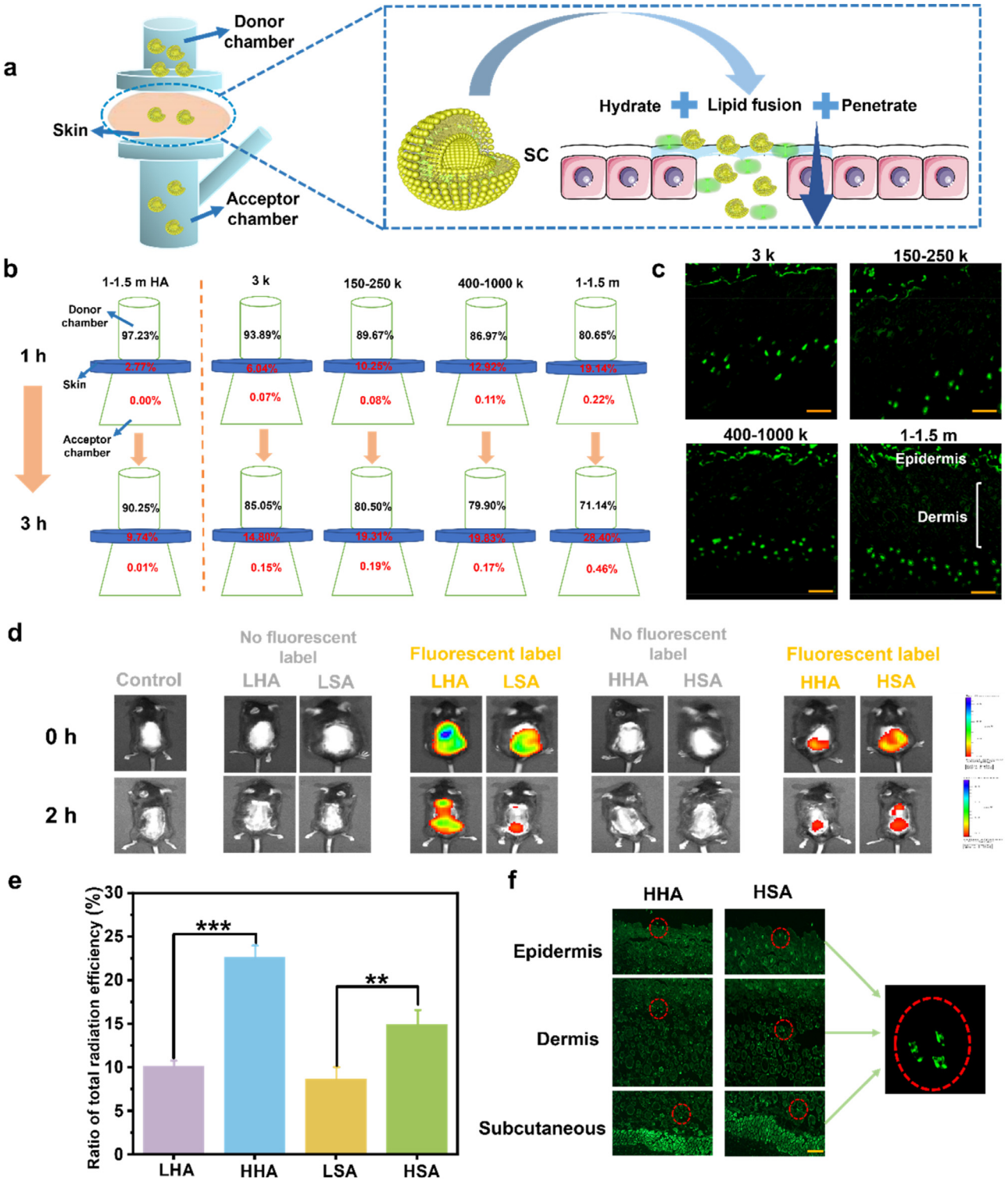

Fig. 2. Kinetic Studies of HA in the Skin. (a) Using Franz diffusion cells to validate the mechanism of hyaluronic acid permeation enhancement by HL. (b) Concentrations of HA in the donor chamber, receiving chamber, and skin for four molecular weights of HL and HA solution with a molecular weight of 1–1.5 m. (c) Penetration and distribution of HL with molecular weights of 3 k, 150–250 k, 400–1000 k, and 1–1.5 m in the skin, scale bar = 100 μm. (d) *In vivo* imaging of small animals with 5AF-labeled high and low molecular weight sodium alginate and hyaluronic acid. (e) Statistical analysis of the fluorescence penetration ratio in the dorsal area of mice 2 h later from (d). (f) Distribution of liposomes containing high molecular weight HA and SA in the dorsal skin of mice, scale bar = 100 μm. $^{*}P < 0.05$; $^{**}P < 0.01$; $^{***}P < 0.001$; $^{****}P < 0.0001$.

delivery. The formation of stable liposome composite structures is crucial for efficient transdermal penetration and treatment [39]. Therefore, this study continuously measured the particle size changes of liposomes with different molecular weights under storage conditions at 4°C over seven days to assess the stability of HL. The Fig. 1e, f showed that there is a certain increase in the particle size of liposomes with different molecular weights. After continuous measurement for 7 days, the particle sizes remain below 500 nm. Simultaneous polydispersity index (PDI) measurements revealed that the PDI of the liposomes remained below 0.3, indicating the absence of aggregation. Therefore, the results above demonstrate that liposomes constructed using HA have a homogeneous particle size distribution and possess persistent stability, meeting the basic requirements for transdermal clinical applications [40].

3.2. Kinetic analysis of hyaluronic acid in skin tissue

To visually observe the kinetics of hyaluronic acid in the skin, this study utilized the absorbance at 486 nm of 5AF to analyze the content of fluorescently modified HA. Initially, a series of HA-5AF liposome solutions of different molecular weights were prepared. Using a multi-functional enzyme reader, the absorbance of hyaluronic acid at different concentrations was measured and recorded. As shown in Supplementary Fig. 1, linear regression was performed with absorbance as the y-axis and solution concentration as the x-axis, yielding regression equations for the concentrations of HA-5AF liposome suspensions. The residence time and quantity of HA in the skin are crucial factors in evaluating the transdermal system. Hence, using Franz diffusion cells and excised mouse back skin tissues, an *in vitro* permeation experiment was conducted to track HA penetration efficiency through the skin. As shown in Fig. 2b, after 1 hour and 3 h, the content of hyaluronic acid was measured. Due to the large molecular structure of HHA, its pure solution was not easily absorbed transdermally, whereas HHL was able to carry more hyaluronic acid molecules into the skin, demonstrating better performance in both skin residence and transdermal penetration. Further, after washing, embedding, and preparing the skin into cryosections, the fluorescence microscopy observations showed (Fig. 2c) that all four molecular weights of hyaluronic acid liposomes had penetrated the skin. The HHL group, due to its larger molecular structure being less susceptible to degradation, exhibited higher fluorescence intensity. This confirms that embedded liposomes can effectively promote the transdermal delivery of hyaluronic acid. To validate from multiple angles that this liposome embedding technique can efficiently facilitate the transdermal delivery of large molecules, live imaging analysis was conducted for fluorescently labeled high molecular weight sodium alginate and hyaluronic acid. The Fig. 2d showed that both high molecular weight SA and HA effectively penetrated the skin. Quantitative analysis of the penetrated fluorescence using living image software revealed that the transdermal penetration ratio of large molecules exceeded 10 % (Fig. 2e). Furthermore, as shown in Fig. 2f, cryosections clearly demonstrated the distribution of large molecular fluorescent liposomes in the epidermis, dermis, and subcutaneous layers of the skin. Therefore, this study

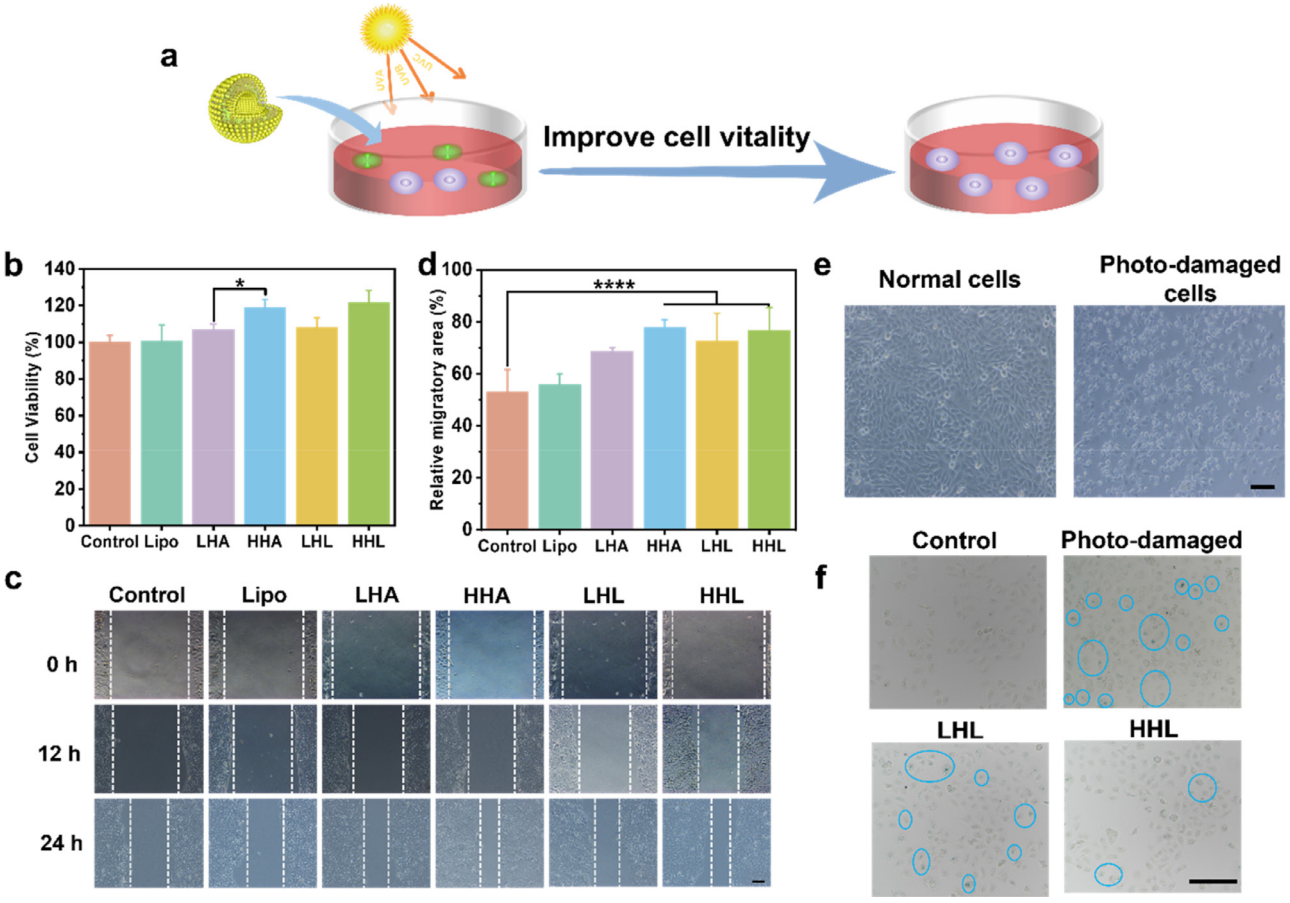

Fig. 3. Study on the effects of HHL on HaCat cells. (a) Schematic diagram of the mechanism by which HHL enhances cell vitality and inhibits aging. (b) Proliferation rates of cells after treatment with Lipo, LHA, HHA, LHL, and HHL. (c) Cell migration images, scale bar = 100 μm. (d) Quantitative analysis of the relative migration areas for each group. (e) HaCat cells in normal condition and after photodamage, scale bar = 50 μm. (f) SA-β-gal staining of HaCat cells treated with LHL and HHL after photodamage, scale bar = 50 μm. $^{*}P < 0.05$; $^{**}P < 0.01$; $^{***}P < 0.001$; $^{****}P < 0.0001$.

innovatively combined fluorescence labeling, live imaging techniques, and other methods to multidimensionally verify that this liposome preparation technique can promote the penetration and long-term residence of large molecular active substances in the skin.

3.3. HHA enhances cell viability and inhibits aging

Human immortalized keratinocytes (HaCat) are widely used for their rapid growth and high survival rate, making them suitable for assessing the moisturizing, antioxidative, and anti-inflammatory effects of materials on skin cells [41]. Therefore, this study explored the effects of HHL on the proliferation and migration of HaCat cells. The cell viability results, as shown in Fig. 3b, indicate that the liposome group without HA did not exhibit cytotoxicity and had proliferation and migration effects comparable to the normal group (normal cell group without added materials), confirming the safety and non-toxicity of the HL preparation process. The proliferation-promoting effects of LHA and HHA on human immortalized keratinocytes after 48 h of treatment were 107.00 % ± 2.98 % and 119.04 % ± 4.19 %, respectively. These results were similar to those of LHL and HHL, further demonstrating that HHL, compared to LHL, exhibited superior cell safety and proliferation-enhancing effects. This provides a cellular-level theoretical basis for the treatment of skin with HHA [42]. Moreover, the cell migration results showed that the reduction in scratch area after 24 h of treatment with LHL (72.8 % ± 10.54 %) and HHL (76.74 % ± 8.71 %) was significantly higher than the control group

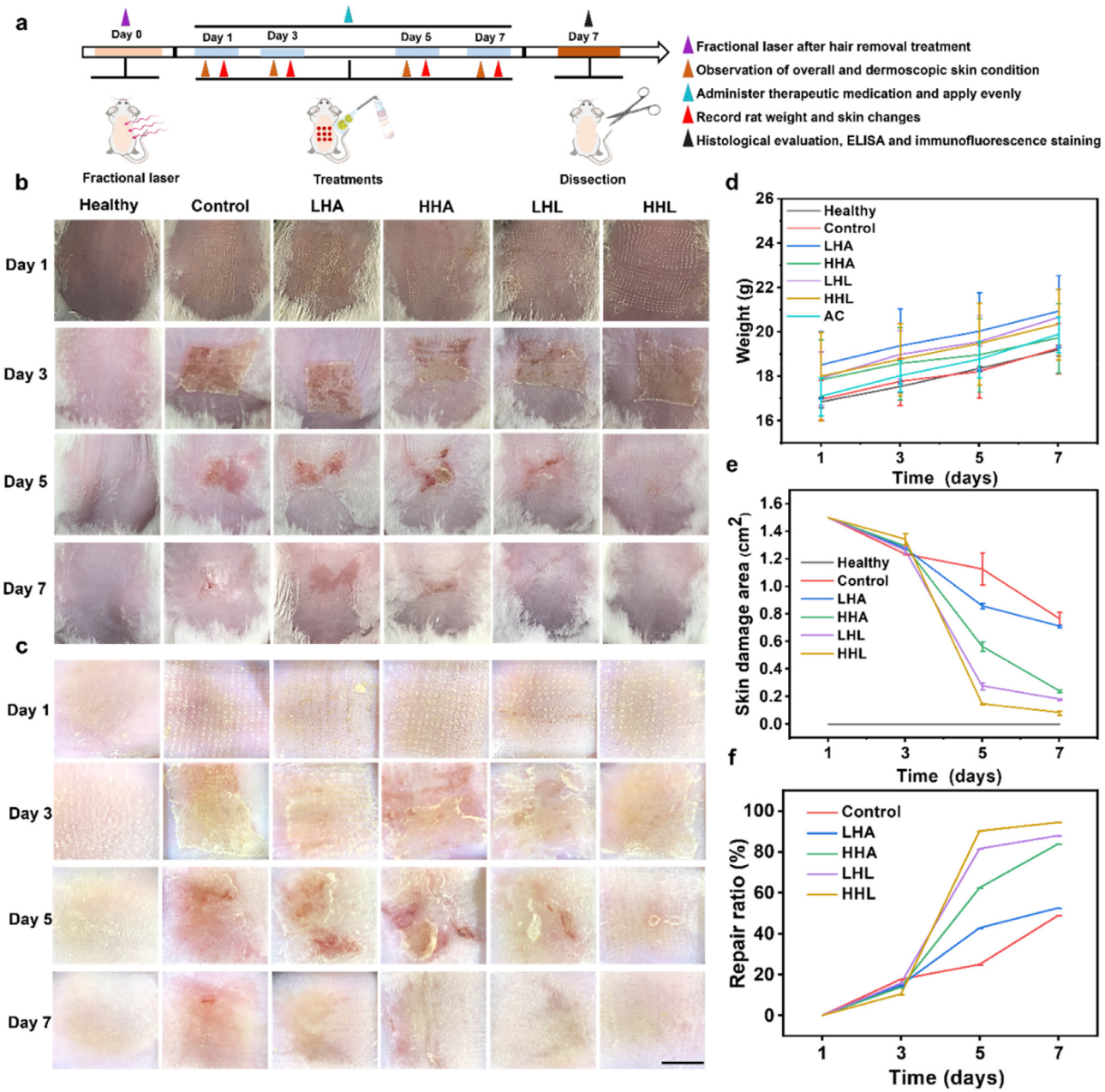

Fig. 4. Overall assessment of the treatment effects on acute skin injury. (a) Establishment of an acute skin injury mouse model and subsequent treatments. (b) Photographs of mice 7 days after fractional laser treatment and application of phosphate-buffered saline, LHA, HHA, LHL, HHL. (c) Dermatoscopic images of the dorsal skin of mice, scale bar = 500 mm. (d) Body weight changes of mice in each group over 7 days. (e) Changes in skin injury area in mice from each group over 7 days. (f) Quantitative analysis of the skin injury repair ratio in mice from each group over 7 days.

(52.9 % ± 8.67 %) (Fig. 3c, d). This conclusion once again proves the advantage of HHA in enhancing skin cell vitality, offering potential for subsequent skin injury treatment [11].SA-β-gal histochemical staining is often used to detect the activity of aging markers in HaCat cells exposed to simulated sunlight [43]. As shown in Fig. 3e, compared to the non-irradiated cells, strong light exposure led to weakened cell adhesion, cell deformation and shrinkage, and increased cytoplasmic content, consistent with previous results [44]. The percentage of senescent cells in non-irradiated cells was low. After irradiation, the percentage of SA-β-gal positive cells increased, and HHL reduced the SA-β-gal activity in irradiated HaCat cells compared to LHL (Fig. 3f). This evidence supports the potential of HHL in enhancing cell viability and mitigating aging effects, especially under conditions of photodamage.

3.4. Overall evaluation of acute skin injury treatment efficacy

In the aforementioned cell experiments, the superiority of high molecular weight hyaluronic acid (HHA) in promoting the proliferation of human keratinocytes was successfully validated. The vitality of keratinocytes plays a crucial role in the repair process of injured skin [45]. To further explore the therapeutic efficacy of HHA in the transdermal system HHL for skin injury, and to validate its clinical application in skin repair, a mouse skin acute injury model induced by laser ablation was established. This study conducted a 7-day treatment, tracking the physiological state of the mice, skin tissue regeneration, and the distribution of hyaluronic acid. At the end of the experiment, pathological sections were collected to evaluate the reparative effects of HHL on acutely injured skin. As shown in Fig. 4d, the weight of mice in all groups increased during the experiment, indicating that the laser ablation acute skin injury model did not affect the normal physiological activities of the mice. The healing process of the mice was observed using a camera and dermatoscope. As shown in Fig. 4b, c, on the day of model establishment, clear lattice wounds were visible on the skin of mice in all groups except the Healthy group. On the third day, a local inflammatory response with skin redness, exudation, and rupture was observed in all groups except the Healthy group. By the fifth day, the redness and rupture of the skin in the Control groups had reduced, with the HHL group showing almost complete disappearance of the wound under dermatoscopy. On the seventh day of treatment, the wounds in the LHL and HHL groups had almost healed, while the Control group, LHA, and HHA groups still had some wounds, as validated by quantitative statistics of skin injury shown in Fig. 4e, f. To explore the utilization of hyaluronic acid during the treatment, the penetration of hyaluronic acid was kinetically analyzed using fluorescent labeling and live imaging. The dorsal skin of the injured mice was removed after 12 h of treatment. As shown in Fig. 5a, b, it was observed that all four materials could effectively penetrate the skin, but quantitative analysis showed that the proportion of fluorescence penetrated by HHL was significantly higher than that of HHA. Skin sections revealed that most of the hyaluronic acid in the LHA and HHA had been degraded, while in the HHL group, the degradation of HHA was slower due to the protective and sustained-release effect of the liposomes (Fig. 5c). This ensured the long-term efficacy of hyaluronic acid, which is more beneficial for the repair of damaged skin.

3.5. HHL promotes inflammation regulation and repair regeneration

Studies have shown that altering inflammation levels can benefit scar reduction and enhance wound healing speed. TNF-α, IL-6, and IL-1β, as three key indicators related to wound inflammation, have garnered extensive attention and research [46]. In this experiment, the content of TNF-α, IL-1β, and IL-6 in mouse skin tissues was measured post-treatment with different materials through an enzyme-linked immunosorbent assay (ELISA). As

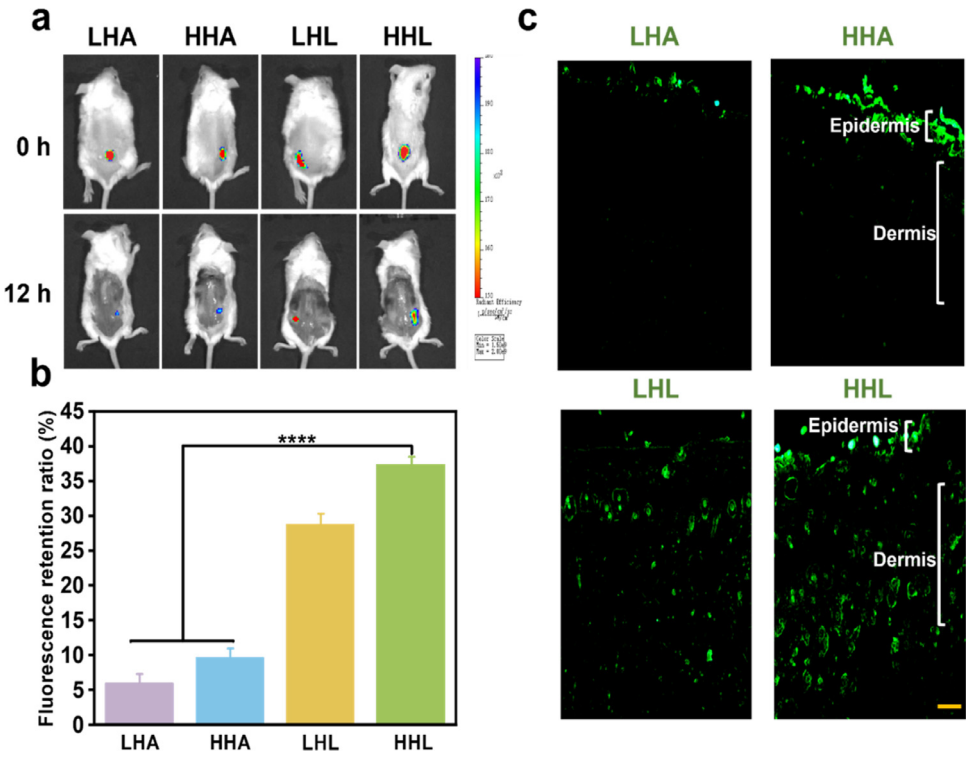

Fig. 5. Penetration of HHL in acutely injured skin. (a) *In vivo* imaging of acute skin injury treated with LHA, HHA, LHL, HHL. (b) Fluorescence quantification in the dorsal skin and muscle tissues of mice. (c) Penetration and distribution of LHA, HHA, LHL, HHL in the skin of live mice, scale bar = 100 μm. $^{*}P < 0.05$; $^{**}P < 0.01$; $^{***}P < 0.001$; $^{****}P < 0.0001$.

shown in Fig. 7d, e, f, the Control group showed the highest levels of TNF-α, IL-1β, and IL-6, indicating an accumulation of inflammatory factors at the site of skin injury in mice. In contrast, the HHL-treated group showed inflammatory factor levels closest to those in Healthy group, indicating a significant reduction in skin inflammation after 7 days of treatment with HHL, achieving levels comparable to the Healthy group and demonstrating outstanding anti-inflammatory effects. Reconstruction of skin-related proteins serves as scaffolding at the injury site to initiate the wound healing processs [47]. H&E staining, Masson staining, and immunohistochemical staining for type III collagen and keratin were used to observe deep tissue repair in mouse skin (Fig. 6a). Compared to the Healthy group, the Control group's epidermal thickness significantly increased, reaching more than four times that of the Healthy group's skin (Fig. 6b). There was a significant decrease in collagen fiber density and the content of type III collagen and keratin (Fig. 6c, d, e). In the treatment groups, the epidermal thickness of the mice gradually decreased, and the density of collagen fibers, type III collagen, and keratin content gradually increased, with the HHL group's indicators being closer to those of the Healthy group. Hence, topical application of HHL significantly reduces the early inflammatory response of wounds and promotes the repair and healing of laser-induced injuries, similar to previous studies on skin injury repair [28]. Ki67 and VEGF, as markers associated with proliferation, play important roles in skin repair. To further verify the proliferative effects of HHL, immunofluorescent staining was used

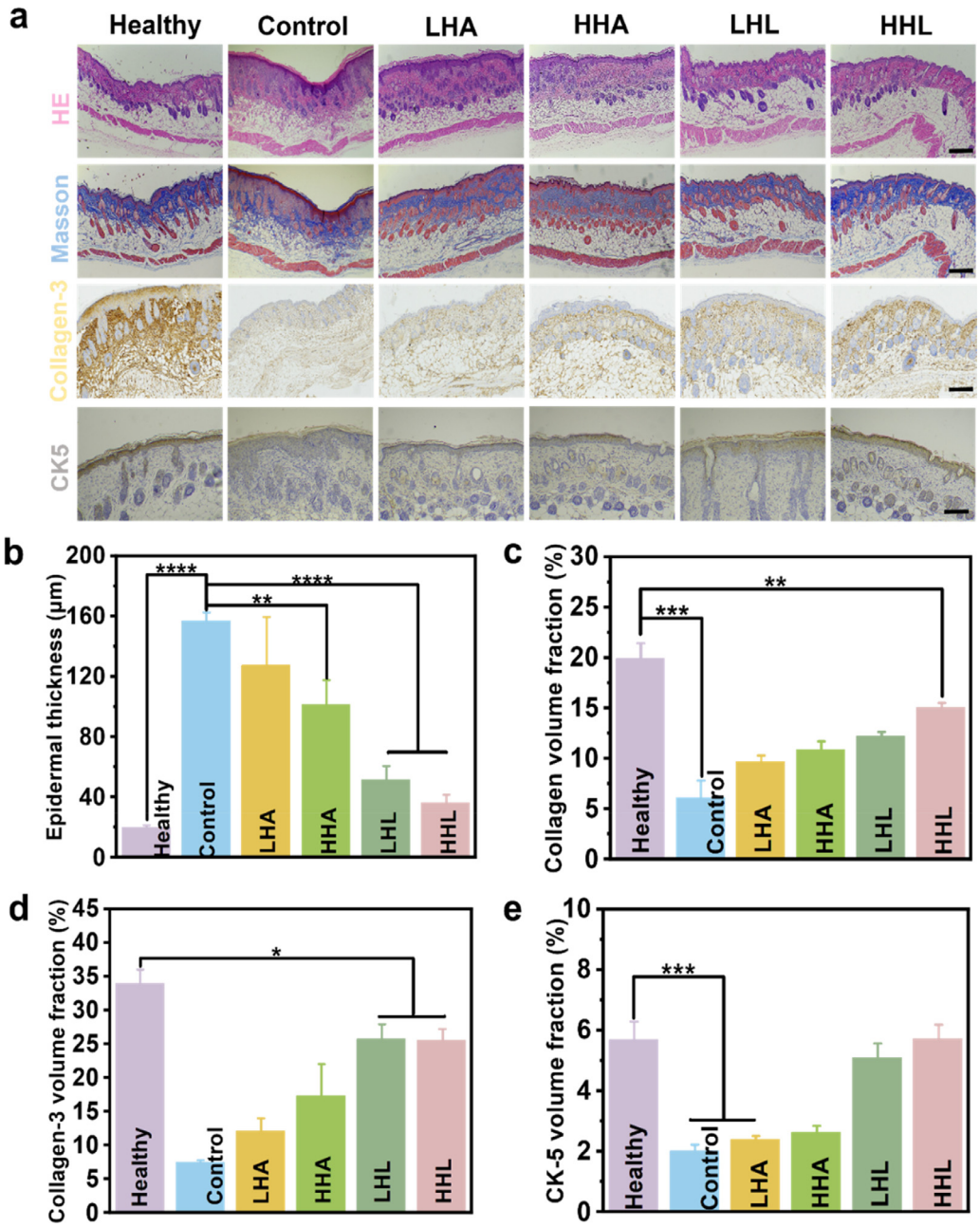

Fig. 6. Histological analysis of scar repair facilitated by HHL. (a) Sequentially from top to bottom: H&E staining, Masson's trichrome staining, immunohistochemical staining for Collagen-3, and immunohistochemical staining for Ck-5, with respective scale bars of 100 μm, 100 μm, 50 μm, 50 μm. (b) Epidermal thickness in each group of mice. (c) Statistical analysis of the collagen volume fraction in the skin of each group of mice. (d) Statistical analysis of the type-3 collagen volume fraction in the skin of each group of mice. (e) Statistical analysis of the CK-5 vol fraction in the skin of each group of mice. $^{*}P < 0.05$; $^{**}P < 0.01$; $^{***}P < 0.001$; $^{****}P < 0.0001$.

to explore the expression of Ki67 and VEGF [48]. As shown in Fig. 7a, c, the Healthy group showed obvious expression of Ki67 and VEGF around skin tissues, indicating robust cell proliferation. The Control group showed lighter staining around hair follicles, with few actively proliferating cells. After treatment with HHL, the expression of Ki67 and VEGF increased, approaching levels in the Healthy group and significantly higher than the Control group. Finally, TUNEL fluorescence staining showed significantly more apoptotic cells in the skin of the Control group, while the HHL group had fewer apoptotic cells, closer to the Healthy group (Fig. 7b). Therefore, this study successfully established an acute photodamage animal model and verified through various evaluation methods that HHL can improve the skin microenvironment, effectively inhibit skin inflammation, and promote the repair and regeneration of injured skin, demonstrating great potential in accelerating skin wound healing.

3.6. Overall evaluation of chronic skin injury treatment efficacy

Excessive ultraviolet radiation can damage the stratum corneum, disrupt the skin barrier, and accelerate skin aging and injury. Previous and current cell experiments have confirmed the potential of HHA in inhibiting skin cell aging. Therefore, to further explore whether the transdermal system HHL can protect the skin and mitigate chronic skin damage caused by simulated sunlight, and to validate its clinical application in daily skin protection, a chronic photodamage model simulating sunlight exposure was established and treated over a period of 60 days. Initially, a preliminary experiment was conducted to determine the minimum erythemal dose (MED) of 500 mj/cm^2 for the mice batch, which served as the standard for changing irradiation energy gradients (as shown in Supplementary Fig. 2). The skin condition of the mice was monitored throughout the treatment process (Supplementary Fig. 3b), along with real-time monitoring of their weight changes (Supplementary Fig. 3a). At the end of

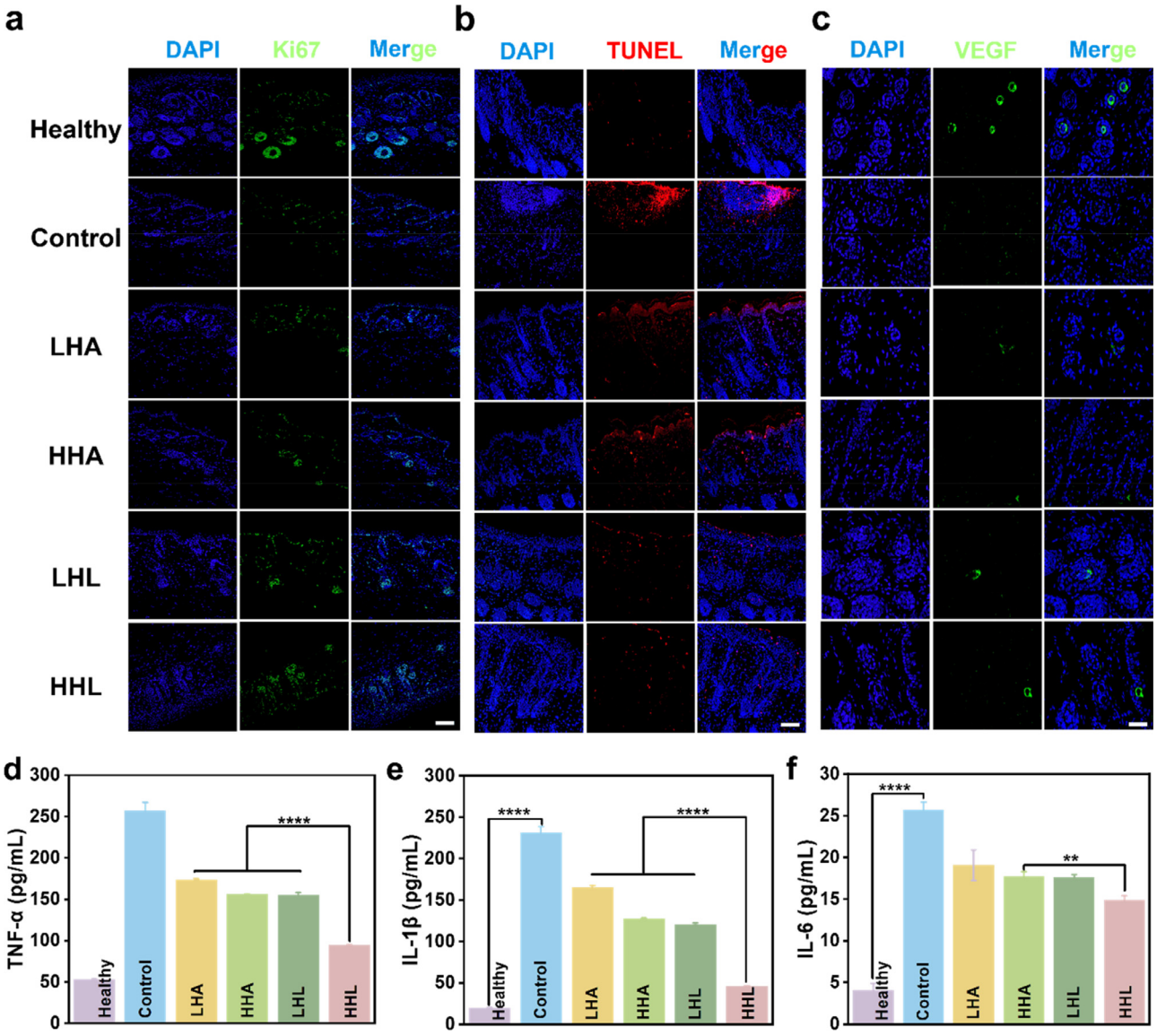

Fig. 7. Evaluation of HHL in Promoting Inflammation Regulation and Regenerative Repair in Mice. (a) Fluorescent expression of Ki67 in the skin of mice from each group, scale bar = 100 μm. (b) Fluorescent expression of Tunel in the skin of mice from each group, scale bar = 100 μm. (c) Fluorescent expression of VEGF in the skin of mice from each group, scale bar = 50 μm. (d) TNF-α levels in the skin of mice from each group. (e) IL-1β levels in the skin of mice from each group. (f) IL-6 levels in the skin of mice from each group. $^{*}P < 0.05$; $^{**}P < 0.01$; $^{***}P < 0.001$; $^{****}P < 0.0001$.

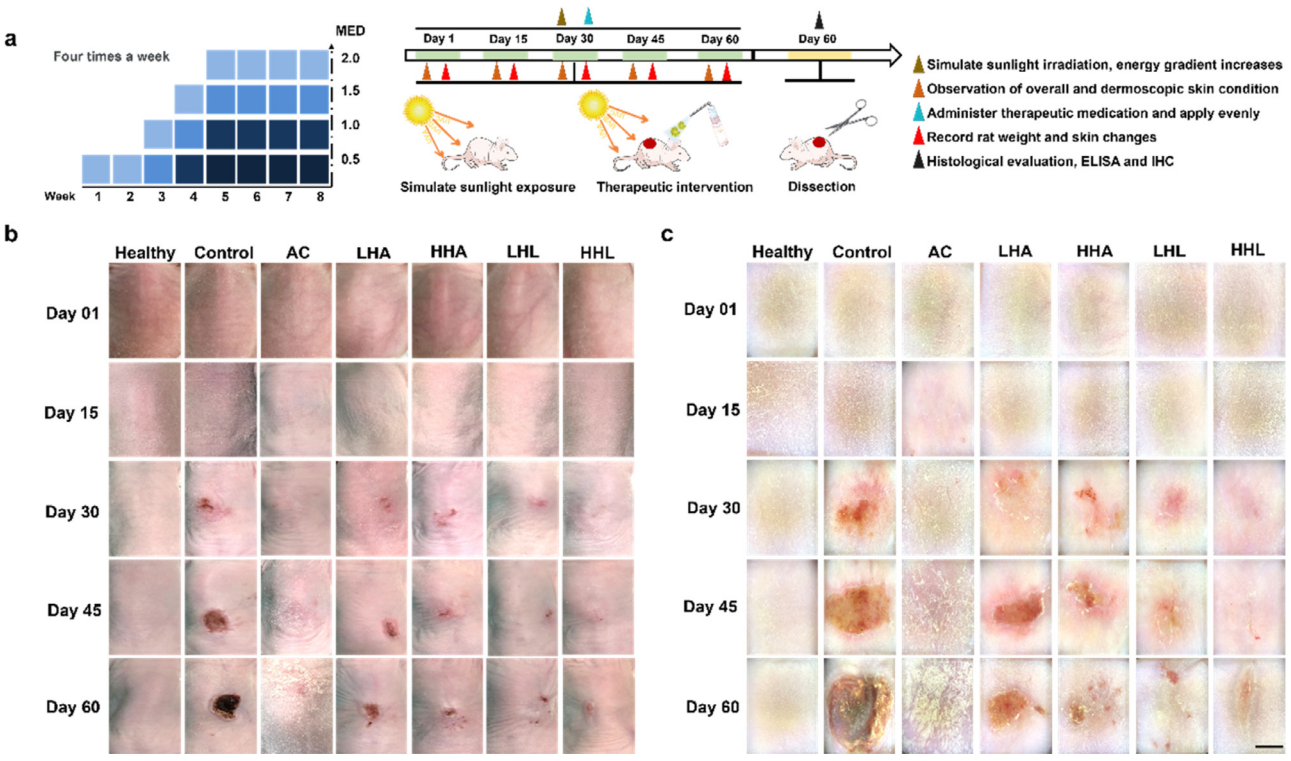

Fig. 8. Overall Evaluation of the Treatment Effects on Chronic Skin Injury. (a) Establishment of a chronic skin injury mouse model and subsequent treatments. (b) Photographs of mice treated with phosphate-buffered saline, retinoic acid cream, LHA, HHA, LHL, HHL for 60 days during simulated sunlight exposure. (c) Dermatoscopic images showing changes in the dorsal skin of mice, scale bar = 500 mm.

the experiment, pathological sections were collected to evaluate the therapeutic effect of HHL on chronic photodamage. As shown in Supplementary Fig. 3a, the weight of mice in all groups increased during the experiment, indicating that the chronic skin damage model did not affect the normal physiological activities of the mice. With increasing amounts of radiation exposure, the skin condition of the mice was observed using a camera and dermatoscope. As shown in Fig. 8b, c, except for the Healthy group and AC group, the skin of the nude mice showed varying degrees of redness, rupture, and wrinkling after thirty days, confirming the successful establishment of the chronic photodamage model. Excitingly, observations and quantitative analysis of the wound area revealed that the HHL group had relatively smaller injury areas, indicating that HHL possesses certain protective functions. Additionally, throughout the experiment, although the injury area in the AC group remained relatively small over time, increasing allergic reactions were observed on their backs, which is a manifestation of drug side effects. In contrast, no allergic reactions were observed in the other groups, highlighting the safety advantages of the transdermal system.

3.7. Histological evaluation of chronic skin injury

Histology of skin tissues elucidates the impact of HHL on changes in back skin structure and collagen deposition. To further understand the therapeutic effects of the transdermal system, H&E staining was first used to determine epidermal thickness. As a quantitative parameter to evaluate the degree of photodamage to the skin, epidermal thickness increases due to skin edema and accumulation of inflammation [28]. As shown in Fig. 9a, b, compared to the Healthy group, the epidermal thickness of the Control group's skin significantly increased, reaching more than five times that of the Healthy group's skin. The HHL group was closest to the Healthy group in this regard. It was also observed that the epidermis of the AC group thickened to a certain extent, possibly related to allergic reactions causing skin peeling and proliferation. Elastic van gieson (EVG) staining was used to investigate the effect of light exposure on collagen fibers. The Fig. 9a, c clearly shows that in the Control group, mouse skin fibers were fractured and disordered, while in the treatment group, collagen fibers were intact. Quantitative analysis revealed that HHL improved the damage to collagen fibers, making them more orderly and providing good protective effects. Matrix metalloproteinases 3 (MMP3), as important indicators of skin damage, mediate the degradation of different components of the extracellular matrix (ECM) and participate in the breakdown of collagen. Therefore, the analysis of MMP3 immunohistochemistry in skin tissues (as shown in Fig. 9a, d) indicated that HHL effectively inhibits the expression of MMP3 during chronic photodamage, thereby reducing the breakdown of collagen and mitigating the harm of photodamage.

3.8. HHL effectively inhibits lipid peroxidation and inflammatory response

Excessive ultraviolet radiation can cause skin oxidative stress, decreased antioxidative capacity, and the onset of inflammatory reactions [49]. In the previously mentioned studies on acute injury, it was found that HHL effectively inhibits the occurrence of inflammatory reactions. This conclusion was re-validated in the treatment of chronic injuries. As shown in Fig. 10d–f, the levels of three important inflammatory indicators, TNF-α, IL-6, and IL-1β, in the HHL-treated mouse tissue were close to those in the Healthy group. The AC group showed increased levels of inflammation due to allergic reactions. Oxidative stress has been proven to play an important role in the development of aging-related diseases. Ultra-

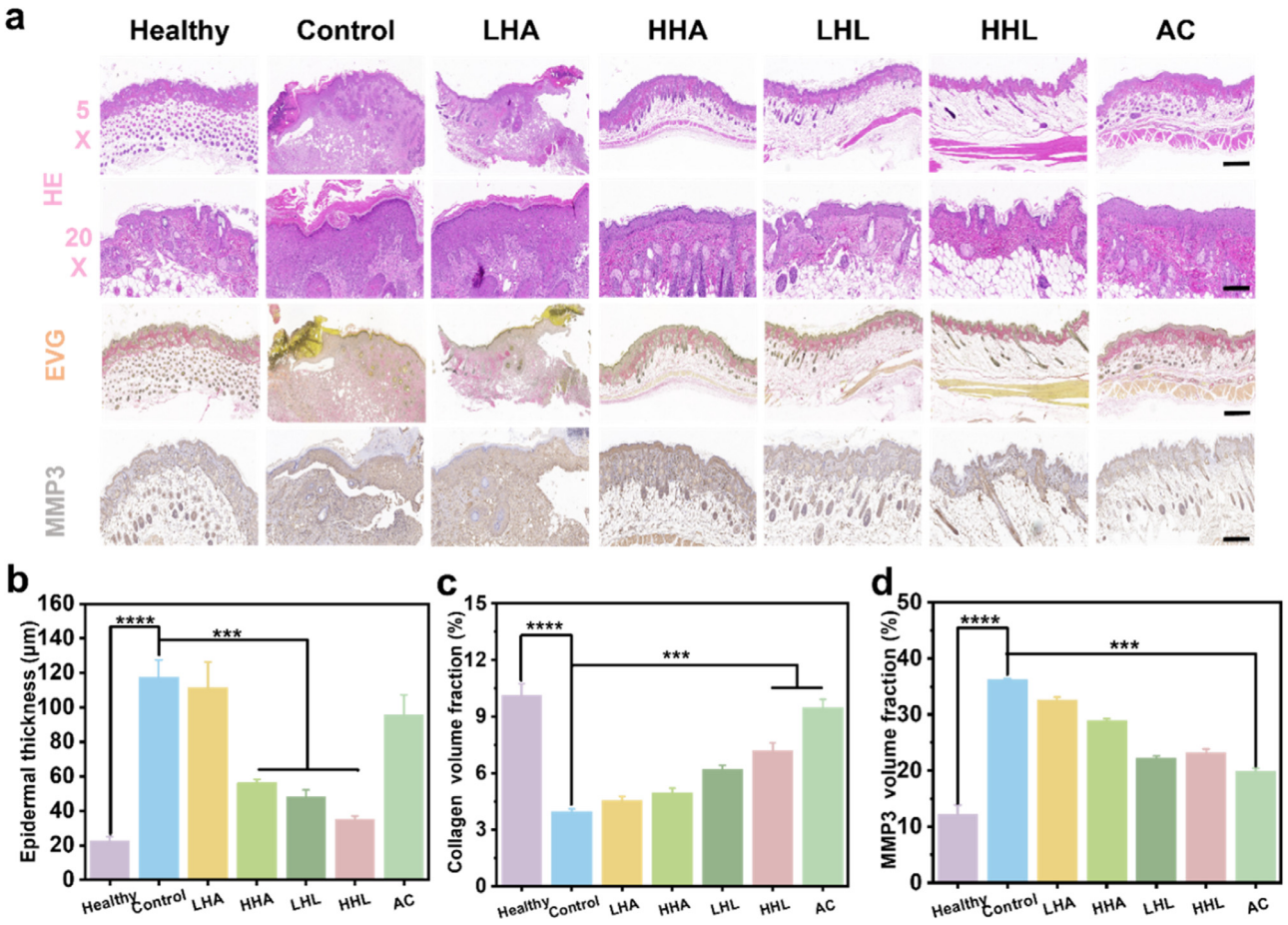

Fig. 9. Histological Analysis of HHL on Chronic Skin Injury. (a) Sequentially from top to bottom: H&E staining, EVG staining, MMP3 immunohistochemical staining, with respective scale bars of 100 μm, 50 μm, 100 μm, 50 μm. (b) Epidermal thickness in each group of mice. (c) Statistical analysis of the collagen volume fraction in the skin of each group of mice. (d) Statistical analysis of the MMP3 vol fraction in the skin of each group of mice. $^{*}P < 0.05$; $^{**}P < 0.01$; $^{***}P < 0.001$; $^{****}P < 0.0001$.

violet radiation can cause cellular aging, leading to oxidative stress. Therefore, the levels of CAT (Catalase), SOD (Superoxide Dismutase), and MDA (Malondialdehyde), which are important parameters reflecting the body's potential antioxidant capacity, were measured using enzyme-linked immunosorbent assays [44]. As shown in Fig. 10a, b, c, the levels of these three indicators in the HHL group were close to those in the Healthy group, significantly inhibiting the accumulation of MDA. It was also observed that the SOD levels in the AC group were relatively low, possibly due to a disruption of some antioxidative functions caused by skin allergic reactions.NF-κB, as an important signaling pathway in oxidative stress and inflammatory responses, influences many downstream proteins upon activation, particularly promoting the expression of inflammation and oxidation-related proteins [28]. Western Blotting results (as shown in Fig. 10g, h) revealed that the Control group had abundant NF-κB expression in the skin, which decreased after treatment, with the HHL group being closest to the Healthy group. This demonstrates the positive regulation of HHL on the NF-κB signaling pathway and its ability to inhibit the intensification of inflammation and oxidation. Therefore, in this experiment, through various evaluations and combining multiple indicators, the advantage of HHL in inhibiting skin oxidative stress and inflammatory responses was proven.

3.9. Analysis of material biocompatibility

Biocompatibility is a critical prerequisite for the biomedical application and subsequent clinical translation of biomaterials. In this study, a commercially available Vitamin A cream was used as a control to evaluate the side effects of the HHL transdermal system on skin conditions and major organs. As shown in Fig. 11a, dermatoscopic observation of the skin condition of mice after three days revealed that the commercially available Vitamin A cream caused dryness and peeling of the mouse skin, while the skin of mice treated with HHL remained smooth and well-moisturized. Further, H&E staining of the heart, liver, spleen, lungs, and kidneys from mice in all experimental groups was performed. As shown in Fig. 11b, no damage or toxicity was observed in the tissues of any group. Additionally, biochemical analysis of serum markers, including liver function (ALT, AST), kidney function (UA, CR), and blood lipids (GLU), was conducted (as shown in Fig. 11c, the number means how many times the indicator content of each group is that of the healthy group). Compared to the Healthy group, all indicators in the treatment groups met standard requirements. Therefore, these results indicate that the transdermal delivery system, constructed by combining liposomes with transdermal properties and hyaluronic acid with multiple functions, exhibits good biocompatibility. This system has potential value for application in clinical practice.

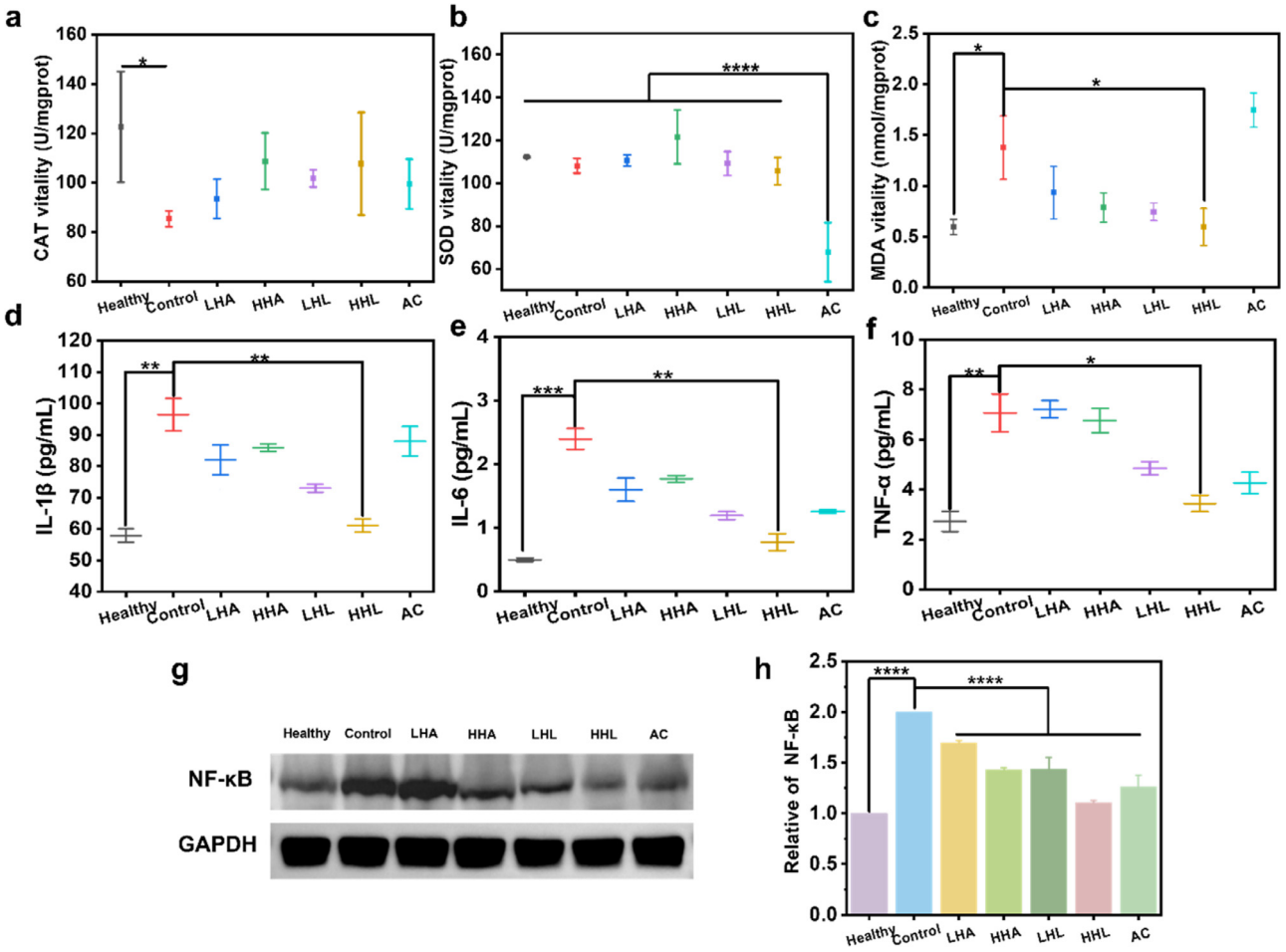

Fig. 10. Evaluation of HHL in Inhibiting Lipid Peroxidation and Inflammatory Response. (a) Expression of CAT activity in the skin of mice from each group. (b) Expression of SOD activity in the skin of mice from each group. (c) Expression of MDA activity in the skin of mice from each group. (d) IL-1β levels in the skin of mice from each group. (e) IL-6 levels in the skin of mice from each group. (f) TNF-α levels in the skin of mice from each group. (g) Western blot (WB) results of NF-κB in the skin of mice from each group. (h) Statistical analysis of the WB results. $^{*}P < 0.05$; $^{**}P < 0.01$; $^{***}P < 0.001$; $^{****}P < 0.0001$.

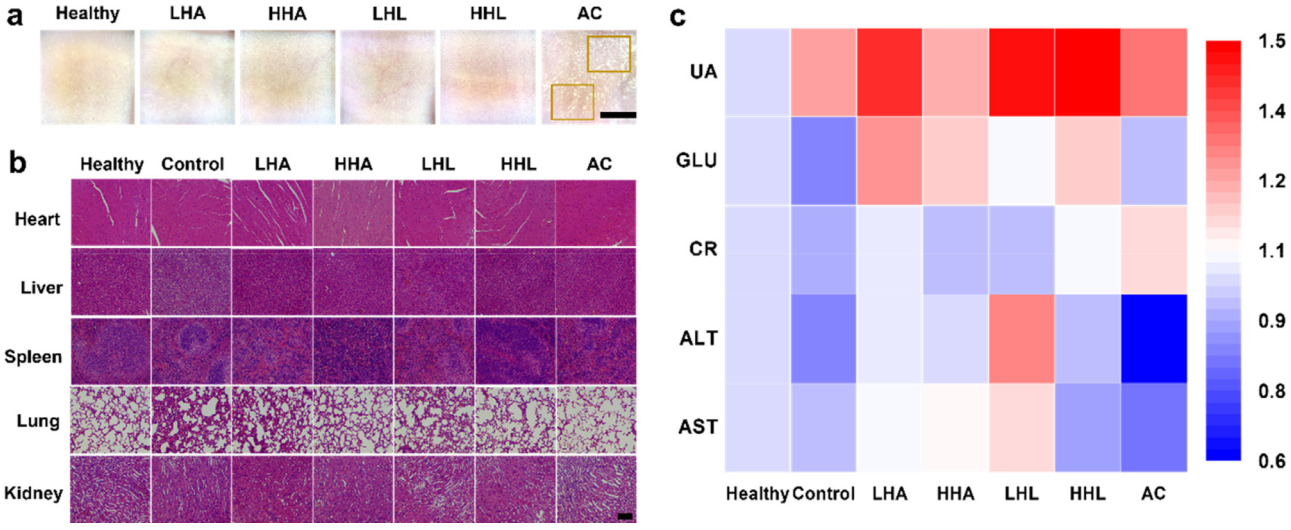

Fig. 11. Evaluation of Material Biosafety. (a) Microscopic view of mouse skin after continuous medication treatment for 3 days. Scale bar = 500 mm. (b) Histopathological examination of the major organs (including heart, liver, spleen, lungs, and kidneys) of mice from different groups. Scale bar = 100 μm. (c) Analysis of blood biochemical parameters including liver function (ALT, AST), kidney function (UA, CR), and blood glucose (GLU) in mice from different groups.

4. Conclusion

In this study, a transdermal system of high molecular weight hyaluronic acid liposomes (HHL) was successfully constructed. By embedding high molecular weight hyaluronic acid (HHA) into the liposome structure, the transdermal utilization rate of HHA was significantly enhanced for the treatment of acute and chronic skin injuries. The system was multidimensionally validated for high penetration and extended retention (EPR) of HHA in the skin using fluorescence labeling and *in vivo* imaging. The experiments on human keratinocytes showed that HHL enhanced cell viability and inhibited cell aging more effectively than other treatments. A laser ablation-induced acute skin injury model was successfully established, where HHL demonstrated significant anti-inflammatory and immunosuppressive properties, promoting skin proliferation and scar repair, thus showing great potential in accelerating skin wound healing. Additionally, a chronic photodamage skin model was developed. HHL markedly improved the skin barrier dysfunction caused by simulated sunlight, inhibited skin redness, inflammatory reactions, and oxidative stress, and promoted collagen expression. A thorough evaluation of the biocompatibility of the material was also conducted, suggesting the potential for integrated therapeutic protection of the skin. Therefore, this transdermal delivery system provides a feasible approach for the non-invasive application of HHA in skin photodamage, holding significant potential for clinical translation and broad application prospects.

Declaration of competing interest

The authors declare that they have no known competing financial interests or personal relationships that could have appeared to influence the work reported in this paper.

CRediT authorship contribution statement

Hui Xing: Data curation, Formal analysis, Investigation, Writing – original draft, Writing – review & editing. **Xiangjun Pan:** Data curation, Formal analysis, Resources, Writing – review & editing. **Yihan Hu:** Data curation, Formal analysis, Writing – review & editing. **Yuhui Yang:** Data curation, Formal analysis. **Ziyi Zhao:** Data curation, Formal analysis. **Huanqi Peng:** Data curation, Formal analysis. **Jianjin Wang:** Data curation, Resources. **Shanying Li:** Data curation, Formal analysis, Resources. **Yunfeng Hu:** Resources, Formal analysis, Funding acquisition. **Guowei Li:** Data curation, Funding acquisition, Writing – original draft, Writing – review & editing. **Dong Ma:** Formal analysis, Funding acquisition, Writing – original draft, Writing – review & editing.

Acknowledgments

This work was financially supported by the National Natural Science Foundation of China (82102113), the Fundamental Research Funds for the Central Universities of Jinan University (21623410), the pilot test of new Hyaluronic Acid Liposomes from Honest Medical China Co., Ltd (ZX20221056).

Supplementary materials

Supplementary material associated with this article can be found, in the online version, at doi:10.1016/j.actbio.2024.05.026.

References

[1] C. Parrado, S. Mercado-Saenz, A. Perez-Davo, Y. Gilaberte, S. Gonzalez, A. Juarranz, Environmental stressors on skin aging. Mechanistic insights, Front. Pharmacol. 10 (2019) 759.
[2] T. Passeron, C. Zouboulis, J. Tan, M. Andersen, R. Katta, X. Lyu, L. Aguilar, D. Kerob, A. Morita, J. Krutmann, Adult skin acute stress responses to short-term environmental and internal aggression from exposome factors, J. Eur. Acad. Dermatol. Venereol. 35 (10) (2021) 1963–1975.
[3] M. El-Domyati, W. Medhat, Minimally invasive facial rejuvenation: current concepts and future expectations, Expert Rev. Dermatol. 8 (5) (2013) 565–580.
[4] A.Z. Alkilani, J. Nasereddin, R. Hamed, S. Nimrawi, G. Hussein, H. Abo-Zour, R.F. Donnelly, Beneath the skin: a review of current trends and future prospects of transdermal drug delivery systems, Pharmaceutics 14 (6) (2022) 1152.
[5] J. Xie, Y. Ji, W. Xue, D. Ma, Y. Hu, Hyaluronic acid-containing ethosomes as a potential carrier for transdermal drug delivery, Colloids Surf. B 172 (2018) 323–329.
[6] D.D. Zhu, Q.L. Wang, X.B. Liu, X.D. Guo, Rapidly separating microneedles for transdermal drug delivery, Acta Biomater. 41 (2016) 312–319.
[7] W.Y. Jeong, M. Kwon, H.E. Choi, K.S. Kim, Recent advances in transdermal drug delivery systems: a review, Biomater. Res. 25 (1) (2021) 24.
[8] P.N. Sudha, M.H. Rose, Beneficial effects of hyaluronic acid, Adv. Food Nutr. Res. 72 (2014) 137–176.
[9] H.S. Jung, K.S. Kim, S.H. Yun, S.K. Hahn, Enhancing the transdermal penetration of nanoconstructs: could hyaluronic acid be the key? Nanomedicine 9 (6) (2014) 743–745.
[10] V.D. Prajapati, P.M. Maheriya, Hyaluronic acid as potential carrier in biomedical and drug delivery applications, in: Functional Polysaccharides for Biomedical Applications, Elsevier, 2019, pp. 213–265.
[11] A.M. Juncan, D.G. Moisă, A. Santini, C. Morgovan, L.-L. Rus, A.L. Vonica-Ţincu, F. Loghin, Advantages of hyaluronic acid and its combination with other bioactive ingredients in cosmeceuticals, Molecules 26 (15) (2021) 4429.
[12] I.S. Bayer, Hyaluronic acid and controlled release: a review, Molecules 25 (11) (2020) 2649.
[13] M.H. Bahrami, S.A. Raeissadat, M. Cheraghi, S. Rahimi-Dehgolan, A. Ebrahimpour, Efficacy of single high-molecular-weight *versus* triple low-molecular-weight hyaluronic acid intra-articular injection among knee osteoarthritis patients, BMC Musculoskelet Disord. 21 (1) (2020) 1–8.
[14] J.-S. Kim, Liposomal drug delivery system, J. Pharm. Investig. 46 (2016) 387–392.
[15] R. Sapkota, A.K. Dash, Liposomes and transferosomes: a breakthrough in topical and transdermal delivery, Ther. Deliv. 12 (2) (2021) 145–158.
[16] S. Siavashy, M. Soltani, M. Ahmadi, B. Landi, H. Mehmanparast, F. Ghorbani-Bidkorbeh, A comprehensive review of one decade of microfluidic platforms applications in synthesis of enhanced carriers utilized in controlled drug delivery, Adv. Mater. Technol. 7 (10) (2022) 2101615.
[17] D. Lombardo, M.A. Kiselev, Methods of liposomes preparation: formation and control factors of versatile nanocarriers for biomedical and nanomedicine application, Pharmaceutics 14 (3) (2022) 543.
[18] M. Ahmadi, S. Siavashy, S.M. Ayyoubzadeh, R. Kecili, F. Ghorbani-Bidkorbeh, Controllable synthesis of polymeric micelles by microfluidic platforms for biomedical applications: a systematic review, Iran. J. Pharm. Res. 20 (2) (2021) 229.
[19] S. Wu, G. Liu, P. Shao, X. Lin, J. Yu, H. Chen, H. Li, S. Feng, Transdermal sustained release properties and anti-photoaging efficacy of liposome-thermosensitive hydrogel system, Adv. Healthc. Mater. (2023) 2301933.
[20] H. Xing, H. Peng, Y. Yang, K. Lv, S. Zhou, X. Pan, J. Wang, Y. Hu, G. Li, D. Ma, Nitric oxide synergizes minoxidil delivered by transdermal hyaluronic acid liposomes for multimodal androgenetic-alopecia therapy, Bioact. Mater. 32 (2024) 190–205.
[21] T. Mohan, R. Kargl, S. Köstler, A. Doliska, G. Findenig, V. Ribitsch, K. Stana-Kleinschek, Functional polysaccharide conjugates for the preparation of microarrays, ACS Appl. Mater. Interfaces 4 (5) (2012) 2743–2751.
[22] M. Kumar, A. Sharma, S. Mahmood, A. Thakur, M.A. Mirza, A. Bhatia, Franz diffusion cell and its implication in skin permeation studies, J. Dispers. Sci. Technol. (2023) 1–14.
[23] Y. Zeng, Y. Song, J. Li, W. Zhang, B. Shi, Visualization and quantification of penetration/mass transfer of acrylic resin retanning agent in leather using florescent tracing technique, J. Am. Leather Chem. Assoc. 111 (11) (2016) 398–405.
[24] N. Annan, A. Borza, L.T. Hansen, Encapsulation in alginate-coated gelatin microspheres improves survival of the probiotic Bifidobacterium adolescentis 15703T during exposure to simulated gastro-intestinal conditions, Food Res. Int. 41 (2) (2008) 184–193.
[25] J. López-García, M. Lehocký, P. Humpolíček, P. Sáha, HaCaT keratinocytes response on antimicrobial atelocollagen substrates: extent of cytotoxicity, cell viability and proliferation, J. Funct. Biomater. 5 (2) (2014) 43–57.
[26] G. Li, K. Lv, X. Pan, S. Zhou, H. Xing, J. Xu, D. Ma, Y. Hu, H. Xu, Dynamic nitric oxide/drug codelivery system based on polyrotaxane architecture for effective treatment of Candida albicans infection, Acta Biomater. 155 (2023) 618–634.
[27] C.-C. Liang, A.Y. Park, J.-L. Guan, *In vitro* scratch assay: a convenient and inexpensive method for analysis of cell migration *in vitro*, Nat. Protoc. 2 (2) (2007) 329–333.
[28] Y. Xie, J. He, S. Li, X. Chen, T. Zhang, Y. Zhao, Y. Lin, X. Cai, A transdermal drug delivery system based on nucleic acid nanomaterials for skin photodamage treatment, Adv. Funct. Mater. 33 (46) (2023) 2303580.
[29] M. Alhajj, M. Zubair, A. Farhana, Enzyme linked Immunosorbent Assay, StatPearls, 2023.
[30] A.B. Santamaria, Molecular Mechanism of PUVA-induced Apoptosis in Mouse Epidermal Cells, The University of Texas School of Public Health, 2001.

[31] Y. Hu, Y. Ma, S. Wu, T. Chen, Y. He, J. Sun, R. Jiao, X. Jiang, Y. Huang, L. Deng, Protective effect of cyanidin-3-O-glucoside against ultraviolet B radiation-induced cell damage in human HaCaT keratinocytes, Front. Pharmacol. 7 (2016) 301.
[32] S. Hu, Z. Li, J. Cores, K. Huang, T. Su, P.-U. Dinh, K. Cheng, Needle-free injection of exosomes derived from human dermal fibroblast spheroids ameliorates skin photoaging, ACS Nano 13 (10) (2019) 11273–11282.
[33] M. Zhang, X. Zhang, T. Tian, Q. Zhang, Y. Wen, J. Zhu, D. Xiao, W. Cui, Y. Lin, Anti-inflammatory activity of curcumin-loaded tetrahedral framework nucleic acids on acute gouty arthritis, Bioact. Mater. 8 (2022) 368–380.
[34] D.D. Verma, S. Verma, G. Blume, A. Fahr, Particle size of liposomes influences dermal delivery of substances into skin, Int. J. Pharm. 258 (1–2) (2003) 141–151.
[35] I. Chauhan, M. Yasir, M. Verma, A.P. Singh, Nanostructured lipid carriers: a groundbreaking approach for transdermal drug delivery, Adv. Pharm. Bull. 10 (2) (2020) 150.
[36] S. Honary, F. Zahir, Effect of zeta potential on the properties of nano-drug delivery systems-a review (Part 1), Trop. J. Pharm. Res. 12 (2) (2013) 255–264.
[37] P. Snetkov, K. Zakharova, S. Morozkina, R. Olekhnovich, M. Uspenskaya, Hyaluronic acid: the influence of molecular weight on structural, physical, physico-chemical, and degradable properties of biopolymer, Polymers 12 (8) (2020) 1800.
[38] S. Karmakar, Particle size distribution and zeta potential based on dynamic light scattering: techniques to characterize stability and surface charge distribution of charged colloids, Recent Trends Mater. Phys. Chem 28 (2019) 117–159.
[39] D.E. Large, R.G. Abdelmessih, E.A. Fink, D.T. Auguste, Liposome composition in drug delivery design, synthesis, characterization, and clinical application, Adv. Drug Deliv. Rev. 176 (2021) 113851.
[40] M.R. Prausnitz, R. Langer, Transdermal drug delivery, Nat. Biotechnol. 26 (11) (2008) 1261–1268.
[41] S.R. Varma, T.O. Sivaprakasam, I. Arumugam, N. Dilip, M. Raghuraman, K. Pavan, M. Rafiq, R. Paramesh, *In vitro* anti-inflammatory and skin protective properties of Virgin coconut oil, J. Tradit. Complement. Med. 9 (1) (2019) 5–14.
[42] Y. Kawano, V. Patrulea, E. Sublet, G. Borchard, T. Iyoda, R. Kageyama, A. Morita, S. Seino, H. Yoshida, O. Jordan, Wound healing promotion by hyaluronic acid: effect of molecular weight on gene expression and *in vivo* wound closure, Pharmaceuticals 14 (4) (2021) 301.
[43] H.K. Kim, Protective effect of garlic on cellular senescence in UVB-exposed HaCaT human keratinocytes, Nutrients 8 (8) (2016) 464.
[44] W. Lu, C. Kong, S. Cheng, X. Xu, J. Zhang, Succinoglycan riclin relieves UVB-induced skin injury with anti-oxidant and anti-inflammatory properties, Int. J. Biol. Macromol. 235 (2023) 123717.
[45] M. Piipponen, D. Li, N.X. Landén, The immune functions of keratinocytes in skin wound healing, Int. J. Mol. Sci. 21 (22) (2020) 8790.
[46] D. Zhou, T. Liu, S. Wang, W. He, W. Qian, G. Luo, Effects of IL-1β and TNF-α on the expression of P311 in vascular endothelial cells and wound healing in mice, Front. Physiol. 11 (2020) 545008.
[47] L. Harsha, M. Brundha, Role of collagen in wound healing, Drug Invent. Today 13 (1) (2020).
[48] Y. Wang, C. Ding, Y. Zhao, J. Zhang, Q. Ding, S. Zhang, N. Wang, J. Yang, S. Xi, T. Zhao, Sodium alginate/poly (vinyl alcohol)/taxifolin nanofiber mat promoting diabetic wound healing by modulating the inflammatory response, angiogenesis, and skin flora, Int. J. Biol. Macromol. 252 (2023) 126530.
[49] D. Fu, J. Huang, K. Li, Y. Chen, Y. He, Y. Sun, Y. Guo, L. Du, Q. Qu, Y. Miao, Dihydrotestosterone-induced hair regrowth inhibition by activating androgen receptor in C57BL6 mice simulates androgenetic alopecia, Biomed. Pharmacother. 137 (2021) 111247.